Computers and Structures 202 (2018) 85–104

Contents lists available at ScienceDirect

Computers and Structures

journal homepage: www.elsevier.com/locate/compstruc

A new 8-node element for analysis of three-dimensional solids

Yeongbin Ko [a], Klaus-Jürgen Bathe [b,*]

[a] 227 Dongil-ro 86, Nowon-gu, Seoul 01618, Republic of Korea
[b] Department of Mechanical Engineering, Massachusetts Institute of Technology, Cambridge, MA 02139, USA

ARTICLE INFO

Article history:
Received 10 January 2018
Accepted 26 February 2018

Keywords:
3D finite element for solids
8-node element
MITC method
EAS method
Incompatible modes
Shear and volumetric locking

ABSTRACT

We propose a new 8-node hexahedral element, the 3D-MITC8 element, for the analysis of three-dimensional solids. We use the MITC method and find the assumed strain field from a thought experiment using a truss idealization. For geometric nonlinear analysis, when needed to suppress hour-glass deformations, the formulation also uses automatically displacement-based contributions to the shear strains. The element shows a much better predictive capability than the displacement-based element. It is computationally more effective than the 8-node element with incompatible modes, and considering accuracy, in linear analysis performs almost as well, and in nonlinear analyses we do not observe spurious instabilities. We show that the new 3D solid element passes all basic tests (the isotropy, zero energy mode and patch tests) and present the finite element solutions of various benchmark problems to illustrate the solution accuracy reached with the new element.

1. Introduction

A three-dimensional 8-node hexahedral solid finite element is frequently employed for the finite element analysis of solids in engineering practice. The element can be used to model many three-dimensional (3D) solids and performs considerably better than the 4-node tetrahedral element. However, the standard 8-node 3D solid element does not satisfy the inf-sup conditions, hence the solution accuracy can severely deteriorate due to shear and volumetric locking [1,2].

To improve the behavior of the standard displacement-based element, additional "incompatible modes" are frequently used [3]. The incompatible modes technique is a special case of the enhanced assumed strain (EAS) method, and the resulting 8-node 3D solid element requires, compared to the standard pure displacement-based element, an additional 9 internal degrees of freedom to represent the conditions of pure bending [3–6]. The element is quite powerful since it alleviates both shear and volumetric locking, but it uses the additional degrees of freedom and can show a non-physical instability in the analyses of nonlinear problems [5–8].

The instability of the EAS elements has been observed to occur in both small and large strain nonlinear analyses [7–14]. If an element mesh is subjected to compression, a spurious hour-glass bending mode may occur in elements eventually resulting into an indefinite stiffness matrix at a certain critical compressive strain [8]. Initially, the hour-glass deformations are small but as they grow, the incremental analysis leads to a spurious collapse of the model.

To treat the spurious instability special solution methods and various element formulations have been developed. The variational principle for nonlinear analysis has been modified, stabilization parameters have been proposed, and mixed-enhanced elements have been developed [9–14], see these references and the references therein. However, further developments are of much interest and, based on our success of developing reliable and efficient shell elements based on the MITC technique [1], we believe that we can also obtain an effective 3D eight-node MITC element.

In this paper we propose a new 8-node hexahedral element based on the standard displacement interpolations and the MITC (Mixed Interpolation of Tensorial Components) approach [1,2,10,15–20]. To obtain a stable element, we choose the tying positions and strain interpolations based on the physical behavior of a simple truss structure that idealizes the 8-node solid element. For geometric nonlinear analysis to suppress hour-glass deformations, the formulation also uses automatically when needed a stabilization scheme based on displacement-based contributions in shear strains. Using these key ideas for the assumed strain field, we find the 3D-MITC8 element to give solution stability, good solution accuracy, and to be computationally efficient. We also extend this element to obtain the 3D-MITC8/1 element based on a mixed displacement-pressure formulation.

* Corresponding author.
E-mail address: kjb@mit.edu (K.J. Bathe).

https://doi.org/10.1016/j.compstruc.2018.02.015
0045-7949/

In the next section we present the concepts we use for the tying and interpolation of the strains in the MITC procedure. Then, in Section 3, we propose the new 3D-MITC8 and 3D-MITC8/1 elements using the total Lagrangian (T.L.) formulation. Of course, the linear behavior corresponds to the first step in the T.L. formulation. Further, in Section 4, the stability and accuracy of the element are assessed using basic tests (the isotropy, zero energy mode and patch tests) and the solutions of various benchmark problems. Finally, in Section 5, we present our conclusions.

2. Tying and interpolation of strains in the MITC procedure

In this section, we present the concepts we employ in the MITC procedure for the new element. The tying positions and interpolations of the assumed strain components are developed considering stability in linear and nonlinear analyses.

The geometry of an 8-node hexahedral solid element is shown in Fig. 1. The element domain is given and the strain components are defined corresponding to the three natural coordinates, r, s and t. For the 3D solid element, there are three normal (in the directions of r, s and t) and three shear (on the planes of rs, st and tr) strain components. The six assumed strain components are denoted by ${}_0\tilde{e}_{rr}$, ${}_0\tilde{e}_{ss}$, ${}_0\tilde{e}_{tt}$, ${}_0\tilde{e}_{rs}$, ${}_0\tilde{e}_{st}$ and ${}_0\tilde{e}_{tr}$.

The choice of assumed strain interpolation must be such that the solid element is stable corresponding to each strain component. To obtain insight, we idealize the hexahedral domain as a truss structure with 8 joints that correspond to the nodes, see Fig. 2(a), of the 8-node 3D element. The selected truss structure is shown in Fig. 2(b). This structure is stable and consists of the minimum number of 2-node truss elements. We next consider the location and direction of each truss element to correspond to an assumed strain component. The location of tying is given by the truss element but to obtain better accuracy using the 3D element in analyses we can move these locations to corresponding Gauss integration points.

If the truss structure we use is stable with the minimum number of truss elements, we can expect that in linear analysis the 3D MITC element will also be stable and will not lock, because a minimum number of truss elements is used. The use of the truss structure to idealize the solid element is similar to how the classical transverse shear assumption was developed by Dvorkin and Bathe for 4-node shell elements, notably for the MITC4 shell element [15]. Here the 4-node shell element transverse shear behavior was idealized by the behavior of four 2-node isoparametric beam elements located along the edges of the shell element, with each beam assuming a constant transverse shear strain [1,15].

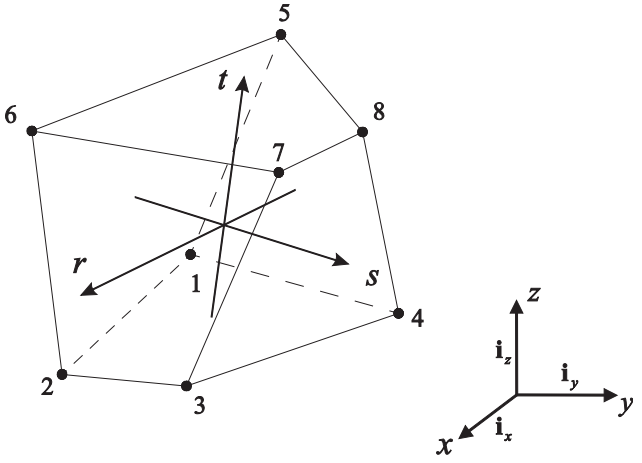

Fig. 1. A standard 8-node hexahedral 3D solid element.

We place a tying location at the center of each truss, and interpolate the assumed strain components according to these locations, see Fig. 2(c). The normal strains (${}_0\tilde{e}_{rr}$, ${}_0\tilde{e}_{ss}$ and ${}_0\tilde{e}_{tt}$) are interpolated bilinearly over the planes defined by their respective tying locations and the shear strains (${}_0\tilde{e}_{rs}$, ${}_0\tilde{e}_{st}$ and ${}_0\tilde{e}_{tr}$) are interpolated linearly between the tying points.

While the resulting assumed strain field yields stability in linear analysis, there is an instability that can arise in nonlinear analysis. The phenomenon has been widely observed for enhanced assumed strain elements when initially regular meshes undergo compression [7–14]. Indeed, for the incompatible modes elements, spurious bending deformations or hour-glass modes are seen at a critical state even in small strains [8]. For an 8-node hexahedral element, possible 2D and 3D hour-glass modes are depicted in Fig. 3(a) and (b), respectively. This behavior occurs if an 8-node element has the ability to express pure bending deformations and the surrounding elements cause mixed behavior of bending and compression. The behavior is possible for the incompatible modes element.

The mechanism of this nonlinear instability was studied by Sussman and Bathe [8], where it was found that a spurious bending deformation occurs when a critical compressive strain state is reached. For the two different kinds of hour-glass modes we treat the potential instabilities separately. We suppress the accumulation of a 3D hour-glass mode by using the incremental displacements to calculate the constant compressive strain. Further, we suppress the 2D hour-glass modes and their coupling to the 3D hour-glass mode by interpolating an additional stabilizing shear strain term bilinearly on the respective planes defined by the mid-points on the edges, see Fig. 3(c).

Incorporating these ideas, the assumed strain field is proposed as

$$\begin{aligned}
{}_0\tilde{e}_{rr} &= A^0_{rr} + A^1_{rr}s + A^2_{rr}t + A^3_{rr}st,\\
{}_0\tilde{e}_{ss} &= A^0_{ss} + A^1_{ss}t + A^2_{ss}r + A^3_{ss}tr,\\
{}_0\tilde{e}_{tt} &= A^0_{tt} + A^1_{tt}r + A^2_{tt}s + A^3_{tt}rs,\\
{}_0\tilde{e}_{rs} &= A^0_{rs} + A^1_{rs}t + S^1_{rs}r + S^2_{rs}s + S^3_{rs}rs,\\
{}_0\tilde{e}_{st} &= A^0_{st} + A^1_{st}r + S^1_{st}s + S^2_{st}t + S^3_{st}st,\\
{}_0\tilde{e}_{tr} &= A^0_{tr} + A^1_{tr}s + S^1_{tr}t + S^2_{tr}r + S^3_{tr}tr,
\end{aligned} \tag{1}$$

in which the A^k_{ij} and S^k_{ij} are the unknown strain coefficients. The constants A^k_{ij} ($k = 0, 1, 2, 3$) and corresponding interpolations allow overall stability in linear and nonlinear analyses. The constants S^k_{ij} ($k = 1, 2, 3$) are designed to automatically suppress 2D hour-glass deformations in nonlinear solutions and are significant only when compressive strain has been accumulated.

3. Formulation of 3D-MITC8 element

We use the left-superscript t to denote the current configuration (or 'time') of the element. We employ the total Lagrangian formulation with the reference configuration at time *0* indicated by the left subscript *0*.

The geometry and displacement of the standard 8-node hexahedral 3D solid element is interpolated by [1]

$$\begin{aligned}
{}^t\mathbf{x} &= \sum_{i=1}^{8} h_i(r,s,t)\,{}^t\mathbf{x}_i\\
&= {}^t x\mathbf{i}_x + {}^t y\mathbf{i}_y + {}^t z\mathbf{i}_z\\
&= [\,{}^t x \quad {}^t y \quad {}^t z\,]^T,
\end{aligned}$$

with ${}^t\mathbf{x}_i = [\,{}^t x_i \quad {}^t y_i \quad {}^t z_i\,]^T$,

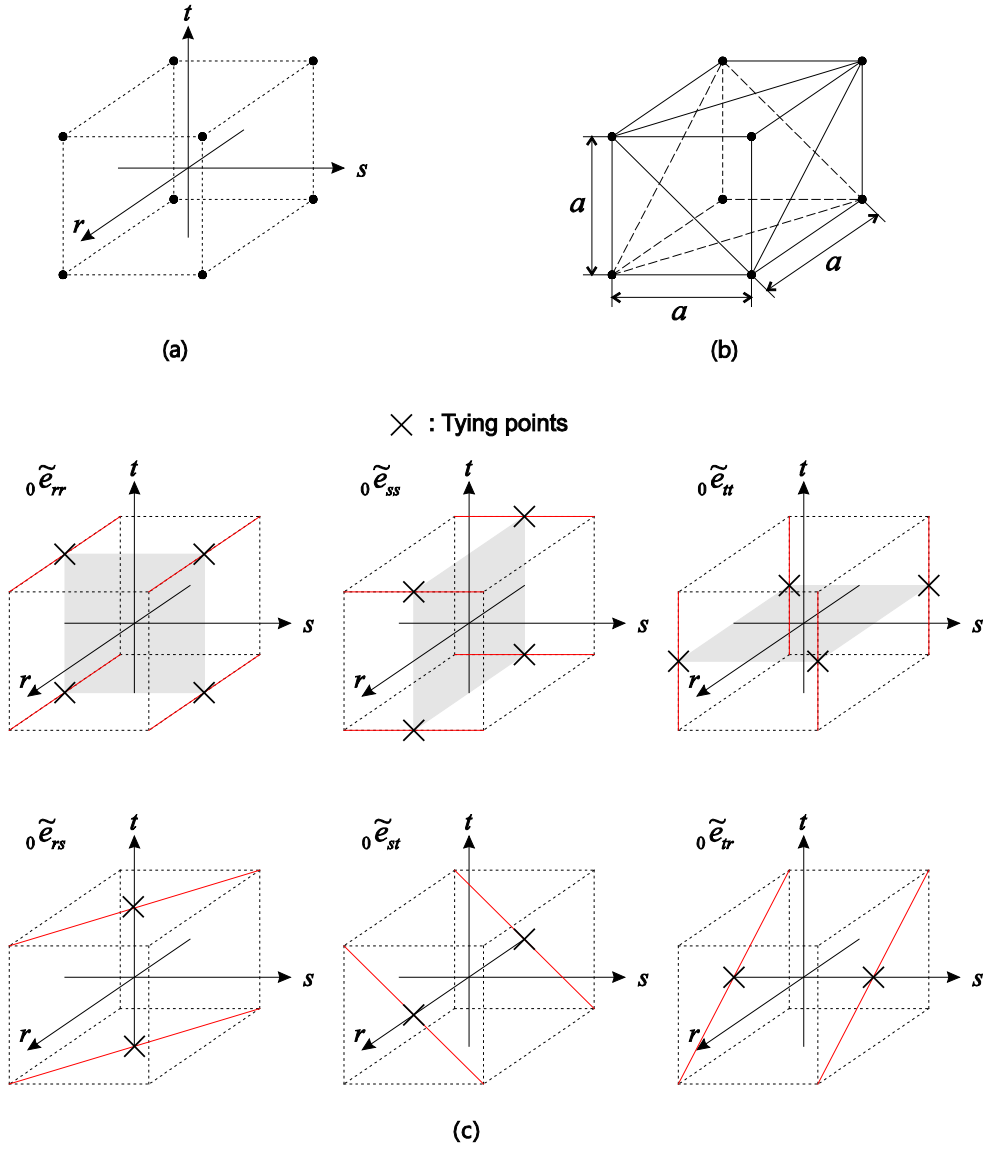

Fig. 2. Identification of tying strains and positions. (a) 8 joints forming a hexahedron. (b) An ideal (minimally stable) truss structure. (c) Tying positions for each assumed strain component.

$$h_i(r,s,t) = \frac{1}{8}(1+\xi_i r)(1+\eta_i s)(1+\zeta_i t),$$

$$\begin{aligned}
&[\xi_1 \quad \xi_2 \quad \xi_3 \quad \xi_4 \quad \xi_5 \quad \xi_6 \quad \xi_7 \quad \xi_8] \\
&\quad = [-1 \quad 1 \quad 1 \quad -1 \quad -1 \quad 1 \quad 1 \quad -1], \\
&[\eta_1 \quad \eta_2 \quad \eta_3 \quad \eta_4 \quad \eta_5 \quad \eta_6 \quad \eta_7 \quad \eta_8] \\
&\quad = [-1 \quad -1 \quad 1 \quad 1 \quad -1 \quad -1 \quad 1 \quad 1], \\
&[\zeta_1 \quad \zeta_2 \quad \zeta_3 \quad \zeta_4 \quad \zeta_5 \quad \zeta_6 \quad \zeta_7 \quad \zeta_8] \\
&\quad = [-1 \quad -1 \quad -1 \quad -1 \quad 1 \quad 1 \quad 1 \quad 1],
\end{aligned} \tag{2}$$

in which $h_i(r,s,t)$ is the standard 8-node interpolation function for the isoparametric procedure, and $\mathbf{i}_x$, $\mathbf{i}_y$, $\mathbf{i}_z$ are base vectors in the global Cartesian coordinate system, see Fig. 1. The incremental displacement vector $\mathbf{u}$ from the configuration at time t to the configuration at time $t+\Delta t$ is

$$\mathbf{u}(r,s,t) = {}^{t+\Delta t}\mathbf{x}(r,s,t) - {}^{t}\mathbf{x}(r,s,t),$$

$$\begin{aligned}
\mathbf{u} &= \sum_{i=1}^{8} h_i(r,s,t)\mathbf{u}_i \\
&= u\mathbf{i}_x + v\mathbf{i}_y + w\mathbf{i}_z \\
&= [u_i \quad v_i \quad w_i]^T
\end{aligned}$$

$$\text{with } \mathbf{u}_i = [u_i \quad v_i \quad w_i]^T. \tag{3}$$

The covariant base vectors and displacement derivatives for the 3D solid element are given as

$$\begin{aligned}
&{}^t\mathbf{g}_r = \frac{\partial\, {}^t\mathbf{x}}{\partial r}, \quad {}^t\mathbf{g}_s = \frac{\partial\, {}^t\mathbf{x}}{\partial s}, \quad {}^t\mathbf{g}_t = \frac{\partial\, {}^t\mathbf{x}}{\partial t}, \quad \mathbf{u}_{,r} = \frac{\partial \mathbf{u}}{\partial r}, \\
&\mathbf{u}_{,s} = \frac{\partial \mathbf{u}}{\partial s}, \quad \mathbf{u}_{,t} = \frac{\partial \mathbf{u}}{\partial t},
\end{aligned} \tag{4}$$

and we define the following 'distortion vectors'

$$\begin{aligned}
&{}^t\mathbf{x}_{rs} = \frac{1}{8}\sum_{i=1}^{8}\xi_i\eta_i\, {}^t\mathbf{x}_i, \quad {}^t\mathbf{x}_{st} = \frac{1}{8}\sum_{i=1}^{8}\eta_i\zeta_i\, {}^t\mathbf{x}_i, \\
&{}^t\mathbf{x}_{tr} = \frac{1}{8}\sum_{i=1}^{8}\zeta_i\xi_i\, {}^t\mathbf{x}_i, \quad {}^t\mathbf{x}_{rst} = \frac{1}{8}\sum_{i=1}^{8}\xi_i\eta_i\zeta_i\, {}^t\mathbf{x}_i,
\end{aligned} \tag{5}$$

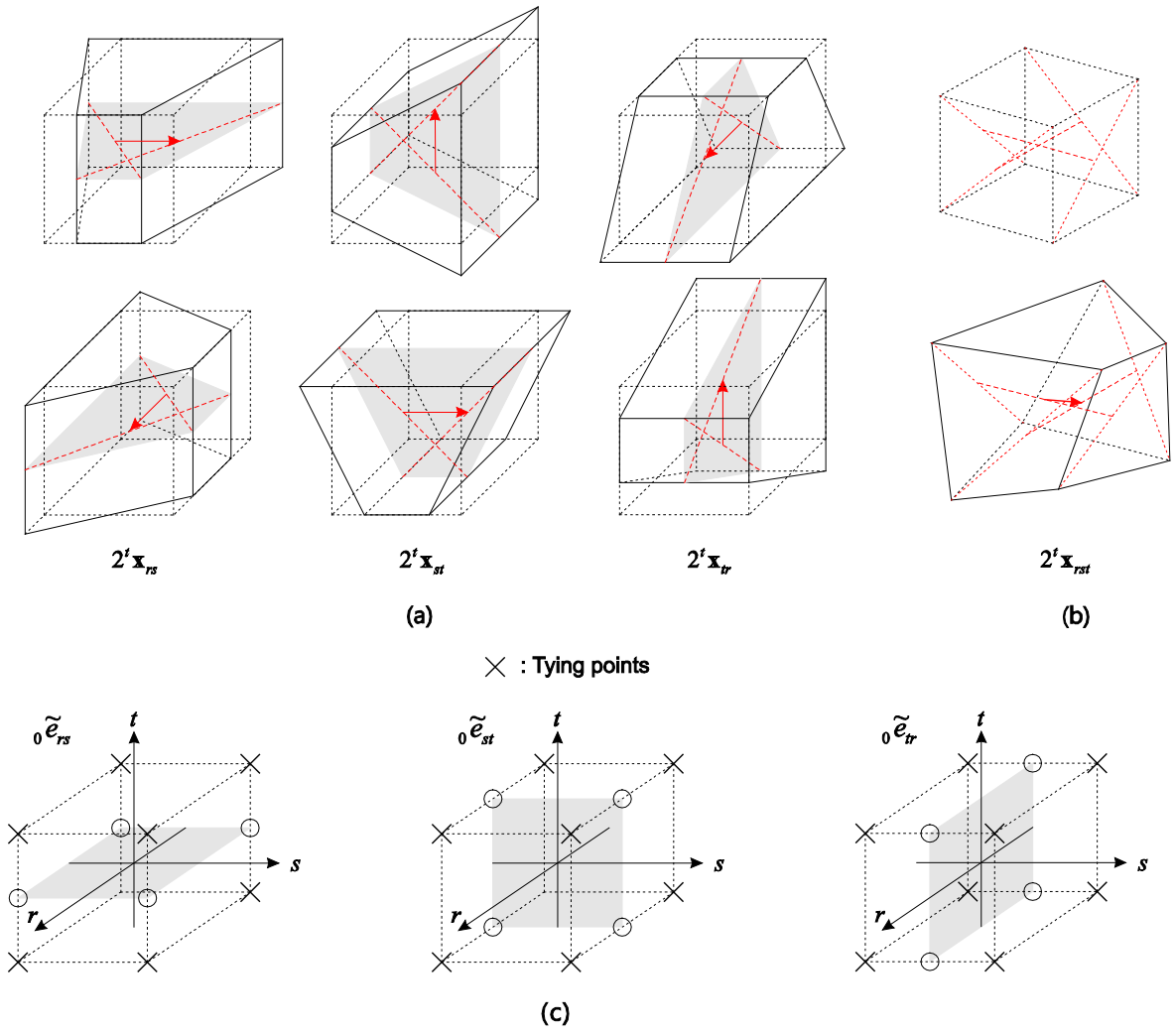

Fig. 3. Identification of tying strains and positions. (a) Two-dimensional hour-glass modes and corresponding distortion vectors. (b) Three-dimensional hour-glass mode and corresponding distortion vector. (c) Tying positions for each assumed strain component.

which measure hour-glass deformations. The three '2D distortion vectors' ${}^t\mathbf{x}_{rs}$, ${}^t\mathbf{x}_{st}$ and ${}^t\mathbf{x}_{tr}$ correspond to 2D deformations, and the '3D distortion vector' ${}^t\mathbf{x}_{rst}$ corresponds to a 3D deformation, see Fig. 3(a) and (b).

We define the following covariant base vectors at the element center,

$$ {}^t\widehat{\mathbf{g}}_i = {}^t\mathbf{g}_i(0,0,0), \text{ with } {}^t\widehat{\mathbf{g}}_1 = {}^t\widehat{\mathbf{g}}_r, {}^t\widehat{\mathbf{g}}_2 = {}^t\widehat{\mathbf{g}}_s, {}^t\widehat{\mathbf{g}}_3 = {}^t\widehat{\mathbf{g}}_t. \tag{6} $$

These three vectors characterize the regular geometry (${}^t\widehat{V}_e$) of the element domain (${}^tV_e$), see Fig. 4.

The seven vectors ${}^t\widehat{\mathbf{g}}_r$, ${}^t\widehat{\mathbf{g}}_s$, ${}^t\widehat{\mathbf{g}}_t$, ${}^t\mathbf{x}_{rs}$, ${}^t\mathbf{x}_{st}$, ${}^t\mathbf{x}_{tr}$ and ${}^t\mathbf{x}_{rst}$ establish the geometry of the 8-node hexahedral element and we define the corresponding incremental displacements from time t to $t+\Delta t$ using

$$ {}^t\mathbf{X}^C = \left[{}^t\widehat{\mathbf{g}}_r \quad {}^t\widehat{\mathbf{g}}_s \quad {}^t\widehat{\mathbf{g}}_t \quad {}^t\mathbf{x}_{rs} \quad {}^t\mathbf{x}_{st} \quad {}^t\mathbf{x}_{tr} \quad {}^t\mathbf{x}_{rst} \right], $$

$$ \mathbf{U}^C = {}^{t+\Delta t}\mathbf{X}^C - {}^t\mathbf{X}^C = [\,\mathbf{u}_r \quad \mathbf{u}_s \quad \mathbf{u}_t \quad \mathbf{u}_{rs} \quad \mathbf{u}_{st} \quad \mathbf{u}_{tr} \quad \mathbf{u}_{rst}\,], \tag{7} $$

where we note that the displacement vectors $\mathbf{u}_r$, $\mathbf{u}_s$, $\mathbf{u}_t$, $\mathbf{u}_{rs}$, $\mathbf{u}_{st}$, $\mathbf{u}_{tr}$ and $\mathbf{u}_{rst}$ are independent of each other.

The contravariant base vectors are obtained from the covariant base vectors using the standard relationship [1]

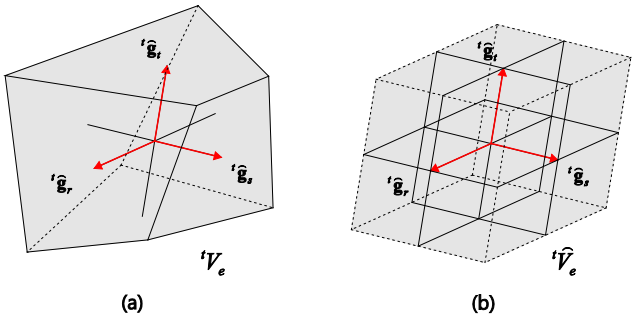

Fig. 4. Characteristic geometry vectors. (a) Three covariant base vectors at the center of the element. (b) The three covariant base vectors characterizing a regular mesh.

$$ {}^t\mathbf{g}_i \cdot {}^t\mathbf{g}^j = \delta_i^j, \text{ with } {}^t\mathbf{g}_1 = {}^t\mathbf{g}_r, \quad {}^t\mathbf{g}_2 = {}^t\mathbf{g}_s, \quad {}^t\mathbf{g}_3 = {}^t\mathbf{g}_t, $$
$$ {}^t\mathbf{g}^1 = {}^t\mathbf{g}^r, \quad {}^t\mathbf{g}^2 = {}^t\mathbf{g}^s, \quad {}^t\mathbf{g}^3 = {}^t\mathbf{g}^t. \tag{8} $$

The covariant Green-Lagrange strain components in the configuration at time t with respect to the reference configuration at time 0 are

$$ {}^{t}_{0}\varepsilon_{ij}(r,s,t) = \frac{1}{2}({}^{t}\mathbf{g}_i \cdot {}^{t}\mathbf{g}_j - {}^{0}\mathbf{g}_i \cdot {}^{0}\mathbf{g}_j). \tag{9} $$

Using Eq. (3) in Eq. (9) applied at time t and $t+\Delta t$, the incremental covariant strain components are

$$ \begin{aligned} {}_{0}\varepsilon_{ij}(r,s,t) &= {}^{t+\Delta t}_{0}\varepsilon_{ij}(r,s,t) - {}^{t}_{0}\varepsilon_{ij}(r,s,t) \\ &= \frac{1}{2}({}^{t}\mathbf{g}_i \cdot \mathbf{u}_{,j} + \mathbf{u}_{,i} \cdot {}^{t}\mathbf{g}_j + \mathbf{u}_{,i} \cdot \mathbf{u}_{,j}), \end{aligned} \tag{10} $$

which can be separated into a linear part (${}_{0}e_{ij}$) and a nonlinear part (${}_{0}\eta_{ij}$)

$$ {}_{0}e_{ij} = \frac{1}{2}({}^{t}\mathbf{g}_i \cdot \mathbf{u}_{,j} + \mathbf{u}_{,i} \cdot {}^{t}\mathbf{g}_j), {}_{0}\eta_{ij} = \frac{1}{2}(\mathbf{u}_{,i} \cdot \mathbf{u}_{,j}), \tag{11} $$

in which ${}^{t}\mathbf{g}_i = \frac{\partial {}^{t}\mathbf{x}}{\partial r_i}$ and $\mathbf{u}_{,i} = \frac{\partial \mathbf{u}}{\partial r_i}$ with $r_1 = r$, $r_2 = s$, $r_3 = t$. Note that ${}_{0}e_{11} = {}_{0}e_{rr}$, ${}_{0}e_{22} = {}_{0}e_{ss}$, ${}_{0}e_{33} = {}_{0}e_{tt}$, ${}_{0}e_{12} = {}_{0}e_{rs}$, ${}_{0}e_{23} = {}_{0}e_{st}$ and ${}_{0}e_{31} = {}_{0}e_{tr}$, and similarly for ${}_{0}\eta_{ij}$.

We use the strain components transformed to a fixed covariant coordinate system defined at the element center in the reference configuration

$$ {}_{0}\widehat{e}_{ij} = {}_{0}e_{kl}g^k_i g^l_j, {}_{0}\widehat{\eta}_{ij} = {}_{0}\eta_{kl}g^k_i g^l_j \text{ with } g^j_i = {}^{0}\widehat{\mathbf{g}}_i \cdot {}^{0}\mathbf{g}^j, \tag{12} $$

and

$$ {}^{0}\lambda(r,s,t) = \frac{{}^{0}j(0,0,0)}{{}^{0}j(r,s,t)} \text{ with } {}^{0}j(r,s,t) = \det\left[{}^{0}\mathbf{g}_r \quad {}^{0}\mathbf{g}_s \quad {}^{0}\mathbf{g}_t\right], \tag{13} $$

as done in previous works [4–6,10,14,16].

We also use the following geometric measure in geometric nonlinear analysis

$$ \begin{aligned} {}^{t}c = &-\left(\sum_{i=1}^{8}\xi_i {}^{t}\mathbf{x}_i\right)\cdot\left(\sum_{i=1}^{8}\xi_i {}^{t}\mathbf{x}_i\right) - \left(\sum_{i=1}^{8}\eta_i {}^{t}\mathbf{x}_i\right)\cdot\left(\sum_{i=1}^{8}\eta_i {}^{t}\mathbf{x}_i\right) \\ &- \left(\sum_{i=1}^{8}\zeta_i {}^{t}\mathbf{x}_i\right)\cdot\left(\sum_{i=1}^{8}\zeta_i {}^{t}\mathbf{x}_i\right), \end{aligned} $$

$$ {}^{t}_{0}c = {}^{t}c - {}^{0}c, \tag{14} $$

where ${}^{t}c$ measures the normal compressive deformation of the hexahedral element and ${}^{t}_{0}c$ accumulates the history of the measure.

In order to correctly account for the element domain (${}^{0}V_e$), we employ the volume-averaged constant incremental strains [16]

$$ {}_{0}\widehat{e}^{con}_{ij} = \frac{1}{{}^{0}V}\int_{{}^{0}V_e} {}_{0}\widehat{e}_{ij}\, d{}^{0}V_e, {}_{0}\widehat{\eta}^{con}_{ij} = \frac{1}{{}^{0}V}\int_{{}^{0}V_e} {}_{0}\widehat{\eta}_{ij}\, d{}^{0}V_e, $$

$$ {}^{0}V = \int_{{}^{0}V_e} d{}^{0}V_e, \tag{15} $$

which results in the same constant strain part as given by the standard 8-node displacement-based element.

We express the 3D distortion vector as

$$ {}^{t}\mathbf{x}_{rst} = {}^{t}d_r\, {}^{t}\widehat{\mathbf{g}}_r + {}^{t}d_s\, {}^{t}\widehat{\mathbf{g}}_s + {}^{t}d_t\, {}^{t}\widehat{\mathbf{g}}_t, \tag{16} $$

with

$$ {}^{t}d_r = {}^{t}\mathbf{x}_{rst} \cdot {}^{t}\widehat{\mathbf{g}}^r, \quad {}^{t}d_s = {}^{t}\mathbf{x}_{rst} \cdot {}^{t}\widehat{\mathbf{g}}^s, \quad {}^{t}d_t = {}^{t}\mathbf{x}_{rst} \cdot {}^{t}\widehat{\mathbf{g}}^t \text{ with } {}^{t}\widehat{\mathbf{g}}_i \cdot {}^{t}\widehat{\mathbf{g}}^j = \delta^j_i, $$

and obtain likewise the corresponding displacement vector

$$ \mathbf{u}_{rst} = {}^{t}d_r\mathbf{u}_r + {}^{t}d_s\mathbf{u}_s + {}^{t}d_t\mathbf{u}_t. \tag{17} $$

In Eq. (17) the 3D distortions are expressed using the regular deformations. To obtain overall stability in nonlinear analysis, the 3D hour-glass deformations need to be suppressed using the constant strain parts. Hence, we use Eq. (17) in Eq. (15) and denote the resulting 'constant strain' as ${}_{0}\tilde{e}^{con}_{ij}$ and ${}_{0}\tilde{\eta}^{con}_{ij}$, see Appendix A for details.

Based on the above considerations, we thus use for the 3D-MITC8 element the assumed incremental linear strains

$$ \begin{aligned} {}_{0}\tilde{e}_{rr} = {}&{}_{0}\tilde{e}^{con}_{rr} \\ &+ \frac{\sqrt{3}}{4}\,{}_{0}\widehat{e}^{\left(0,\frac{1}{\sqrt{3}},\frac{1}{\sqrt{3}}\right)}_{rr}\,{}^{0}\lambda(r,s,t)\left(s+t+\sqrt{3}st\right) \\ &+ \frac{\sqrt{3}}{4}\,{}_{0}\widehat{e}^{\left(0,-\frac{1}{\sqrt{3}},-\frac{1}{\sqrt{3}}\right)}_{rr}\,{}^{0}\lambda(r,s,t)\left(-s-t+\sqrt{3}st\right) \\ &+ \frac{\sqrt{3}}{4}\,{}_{0}\widehat{e}^{\left(0,\frac{1}{\sqrt{3}},-\frac{1}{\sqrt{3}}\right)}_{rr}\,{}^{0}\lambda(r,s,t)\left(s-t-\sqrt{3}st\right) \\ &+ \frac{\sqrt{3}}{4}\,{}_{0}\widehat{e}^{\left(0,-\frac{1}{\sqrt{3}},\frac{1}{\sqrt{3}}\right)}_{rr}\,{}^{0}\lambda(r,s,t)\left(-s+t-\sqrt{3}st\right), \end{aligned} $$

$$ \begin{aligned} {}_{0}\tilde{e}_{ss} = {}&{}_{0}\tilde{e}^{con}_{ss} \\ &+ \frac{\sqrt{3}}{4}\,{}_{0}\widehat{e}^{\left(\frac{1}{\sqrt{3}},0,\frac{1}{\sqrt{3}}\right)}_{ss}\,{}^{0}\lambda(r,s,t)\left(t+r+\sqrt{3}tr\right) \\ &+ \frac{\sqrt{3}}{4}\,{}_{0}\widehat{e}^{\left(-\frac{1}{\sqrt{3}},0,-\frac{1}{\sqrt{3}}\right)}_{ss}\,{}^{0}\lambda(r,s,t)\left(-t-r+\sqrt{3}tr\right) \\ &+ \frac{\sqrt{3}}{4}\,{}_{0}\widehat{e}^{\left(\frac{1}{\sqrt{3}},0,-\frac{1}{\sqrt{3}}\right)}_{ss}\,{}^{0}\lambda(r,s,t)\left(-t+r-\sqrt{3}tr\right) \\ &+ \frac{\sqrt{3}}{4}\,{}_{0}\widehat{e}^{\left(-\frac{1}{\sqrt{3}},0,\frac{1}{\sqrt{3}}\right)}_{ss}\,{}^{0}\lambda(r,s,t)\left(t-r-\sqrt{3}tr\right), \end{aligned} $$

$$ \begin{aligned} {}_{0}\tilde{e}_{tt} = {}&{}_{0}\tilde{e}^{con}_{tt} \\ &+ \frac{\sqrt{3}}{4}\,{}_{0}\widehat{e}^{\left(\frac{1}{\sqrt{3}},\frac{1}{\sqrt{3}},0\right)}_{tt}\,{}^{0}\lambda(r,s,t)\left(r+s+\sqrt{3}rs\right) \\ &+ \frac{\sqrt{3}}{4}\,{}_{0}\widehat{e}^{\left(-\frac{1}{\sqrt{3}},-\frac{1}{\sqrt{3}},0\right)}_{tt}\,{}^{0}\lambda(r,s,t)\left(-r-s+\sqrt{3}rs\right) \\ &+ \frac{\sqrt{3}}{4}\,{}_{0}\widehat{e}^{\left(\frac{1}{\sqrt{3}},-\frac{1}{\sqrt{3}},0\right)}_{tt}\,{}^{0}\lambda(r,s,t)\left(r-s-\sqrt{3}rs\right) \\ &+ \frac{\sqrt{3}}{4}\,{}_{0}\widehat{e}^{\left(-\frac{1}{\sqrt{3}},\frac{1}{\sqrt{3}},0\right)}_{tt}\,{}^{0}\lambda(r,s,t)\left(-r+s-\sqrt{3}rs\right), \end{aligned} $$

$$ \begin{aligned} {}_{0}\tilde{e}_{rs} = {}&{}_{0}\tilde{e}^{con}_{rs} + \frac{1}{2}\left({}_{0}\widehat{e}^{(0,0,1)}_{rs} - {}_{0}\widehat{e}^{(0,0,-1)}_{rs}\right){}^{0}\lambda(r,s,t)t \\ &+ \tanh({}^{t}_{0}c)\,{}_{0}\widehat{e}^{stab}_{rs}(r,s)\,{}^{0}\lambda(r,s,t), \end{aligned} $$

$$ \begin{aligned} {}_{0}\tilde{e}_{st} = {}&{}_{0}\tilde{e}^{con}_{st} + \frac{1}{2}\left({}_{0}\widehat{e}^{(1,0,0)}_{st} - {}_{0}\widehat{e}^{(-1,0,0)}_{st}\right){}^{0}\lambda(r,s,t)r \\ &+ \tanh({}^{t}_{0}c)\,{}_{0}\widehat{e}^{stab}_{st}(s,t)\,{}^{0}\lambda(r,s,t), \end{aligned} $$

$$ \begin{aligned} {}_{0}\tilde{e}_{tr} = {}&{}_{0}\tilde{e}^{con}_{tr} + \frac{1}{2}({}_{0}\widehat{e}^{(0,1,0)}_{tr} - {}_{0}\widehat{e}^{(0,-1,0)}_{tr}){}^{0}\lambda(r,s,t)s \\ &+ \tanh({}^{t}_{0}c)\,{}_{0}\widehat{e}^{stab}_{tr}(t,r)\,{}^{0}\lambda(r,s,t), \end{aligned} \tag{18a} $$

$$ \begin{aligned} {}_{0}\widehat{e}^{stab}_{rs} = {}&\frac{\sqrt{3}}{8}\left({}_{0}\widehat{e}^{\left(\frac{1}{\sqrt{3}},\frac{1}{\sqrt{3}},1\right)}_{rs} + {}_{0}\widehat{e}^{\left(\frac{1}{\sqrt{3}},\frac{1}{\sqrt{3}},-1\right)}_{rs}\right)\left(r+s+\sqrt{3}rs\right) \\ &+ \frac{\sqrt{3}}{8}\left({}_{0}\widehat{e}^{\left(-\frac{1}{\sqrt{3}},-\frac{1}{\sqrt{3}},1\right)}_{rs} + {}_{0}\widehat{e}^{\left(-\frac{1}{\sqrt{3}},-\frac{1}{\sqrt{3}},-1\right)}_{rs}\right)\left(-r-s+\sqrt{3}rs\right) \\ &+ \frac{\sqrt{3}}{8}\left({}_{0}\widehat{e}^{\left(\frac{1}{\sqrt{3}},-\frac{1}{\sqrt{3}},1\right)}_{rs} + {}_{0}\widehat{e}^{\left(\frac{1}{\sqrt{3}},-\frac{1}{\sqrt{3}},-1\right)}_{rs}\right)\left(r-s-\sqrt{3}rs\right) \\ &+ \frac{\sqrt{3}}{8}\left({}_{0}\widehat{e}^{\left(-\frac{1}{\sqrt{3}},\frac{1}{\sqrt{3}},1\right)}_{rs} + {}_{0}\widehat{e}^{\left(-\frac{1}{\sqrt{3}},\frac{1}{\sqrt{3}},-1\right)}_{rs}\right)\left(-r+s-\sqrt{3}rs\right), \end{aligned} $$

$$
\begin{aligned}
{}_0\widehat{e}_{st}^{stab} = {} & \frac{\sqrt{3}}{8}\left({}_0\widehat{e}_{st}^{\left(1,\frac{1}{\sqrt{3}},\frac{1}{\sqrt{3}}\right)} + {}_0\widehat{e}_{st}^{\left(-1,\frac{1}{\sqrt{3}},\frac{1}{\sqrt{3}}\right)}\right)\left(s+t+\sqrt{3}st\right) \\
& + \frac{\sqrt{3}}{8}\left({}_0\widehat{e}_{st}^{\left(1,-\frac{1}{\sqrt{3}},-\frac{1}{\sqrt{3}}\right)} + {}_0\widehat{e}_{st}^{\left(-1,-\frac{1}{\sqrt{3}},-\frac{1}{\sqrt{3}}\right)}\right)\left(-s-t+\sqrt{3}st\right) \\
& + \frac{\sqrt{3}}{8}\left({}_0\widehat{e}_{st}^{\left(1,\frac{1}{\sqrt{3}},-\frac{1}{\sqrt{3}}\right)} + {}_0\widehat{e}_{st}^{\left(-1,\frac{1}{\sqrt{3}},-\frac{1}{\sqrt{3}}\right)}\right)\left(s-t-\sqrt{3}st\right) \\
& + \frac{\sqrt{3}}{8}\left({}_0\widehat{e}_{st}^{\left(1,-\frac{1}{\sqrt{3}},\frac{1}{\sqrt{3}}\right)} + {}_0\widehat{e}_{st}^{\left(-1,-\frac{1}{\sqrt{3}},\frac{1}{\sqrt{3}}\right)}\right)\left(-s+t-\sqrt{3}st\right),
\end{aligned}
$$

$$
\begin{aligned}
{}_0\widehat{e}_{tr}^{stab} = {} & \frac{\sqrt{3}}{8}\left({}_0\widehat{e}_{tr}^{\left(\frac{1}{\sqrt{3}},1,\frac{1}{\sqrt{3}}\right)} + {}_0\widehat{e}_{tr}^{\left(\frac{1}{\sqrt{3}},-1,\frac{1}{\sqrt{3}}\right)}\right)\left(t+r+\sqrt{3}tr\right) \\
& + \frac{\sqrt{3}}{8}\left({}_0\widehat{e}_{tr}^{\left(-\frac{1}{\sqrt{3}},1,-\frac{1}{\sqrt{3}}\right)} + {}_0\widehat{e}_{tr}^{\left(-\frac{1}{\sqrt{3}},-1,-\frac{1}{\sqrt{3}}\right)}\right)\left(-t-r+\sqrt{3}tr\right) \\
& + \frac{\sqrt{3}}{8}\left({}_0\widehat{e}_{tr}^{\left(\frac{1}{\sqrt{3}},1,-\frac{1}{\sqrt{3}}\right)} + {}_0\widehat{e}_{tr}^{\left(\frac{1}{\sqrt{3}},-1,-\frac{1}{\sqrt{3}}\right)}\right)\left(-t+r-\sqrt{3}tr\right) \\
& + \frac{\sqrt{3}}{8}\left({}_0\widehat{e}_{tr}^{\left(-\frac{1}{\sqrt{3}},1,\frac{1}{\sqrt{3}}\right)} + {}_0\widehat{e}_{tr}^{\left(-\frac{1}{\sqrt{3}},-1,\frac{1}{\sqrt{3}}\right)}\right)\left(t-r-\sqrt{3}tr\right),
\end{aligned}
\tag{18b}
$$

in which the superscript '*stab*' denotes the strain terms obtained directly from the displacements for stabilizing the spurious hourglass modes. These strain terms are multiplied by the function *tanh* $\left({}_0^t c\right)$ and hence the effect of stabilization is maximum at large compressive deformations. In linear analysis there is no accumulated

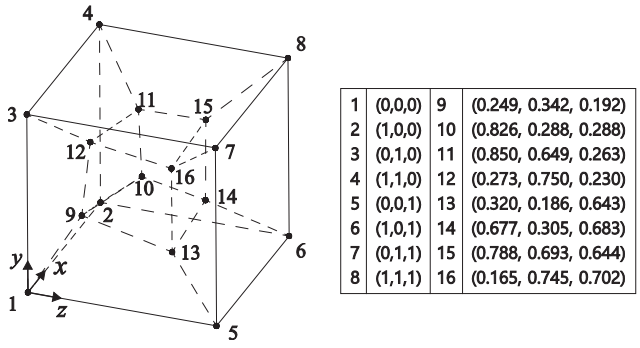

1	(0,0,0)	9	(0.249, 0.342, 0.192)
2	(1,0,0)	10	(0.826, 0.288, 0.288)
3	(0,1,0)	11	(0.850, 0.649, 0.263)
4	(1,1,0)	12	(0.273, 0.750, 0.230)
5	(0,0,1)	13	(0.320, 0.186, 0.643)
6	(1,0,1)	14	(0.677, 0.305, 0.683)
7	(0,1,1)	15	(0.788, 0.693, 0.644)
8	(1,1,1)	16	(0.165, 0.745, 0.702)

Fig. 5. Mesh used for the patch test.

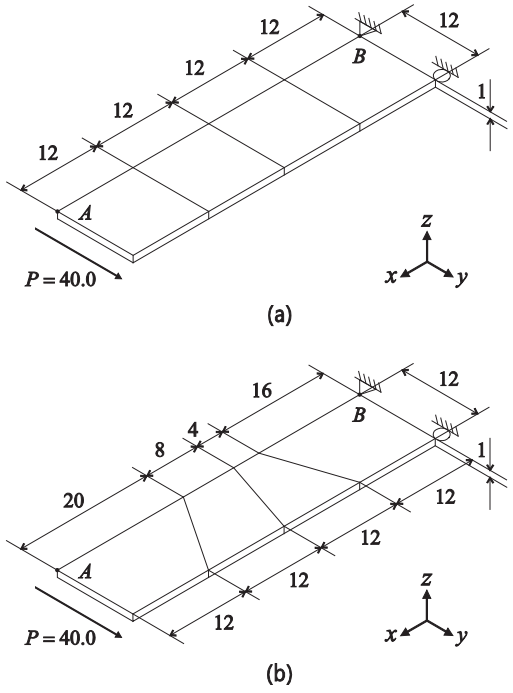

Fig. 6. Cantilever problem (1×4 mesh, $E = 3.0 \times 10^4$ and $\nu = 0.0$). (a) Regular mesh. (b) Distorted mesh.

Table 1
Predicted *y*-displacement at the tip (point A) in the cantilever problem.

Elements	Regular mesh	Distorted mesh
H8	0.235611	0.204659
H8I9	0.347833	0.345307
3D-MITC8	0.347833	0.304211
Exact solution	0.347833	

Table 2
Predicted stress-*xx* ($\times 10^2$) at the support (point B) in the cantilever problem.

Elements	Regular mesh	Distorted mesh
H8	0.466667	0.351417
H8I9	0.700000	0.618222
3D-MITC8	0.700000	0.580764
Exact solution	0.700000	

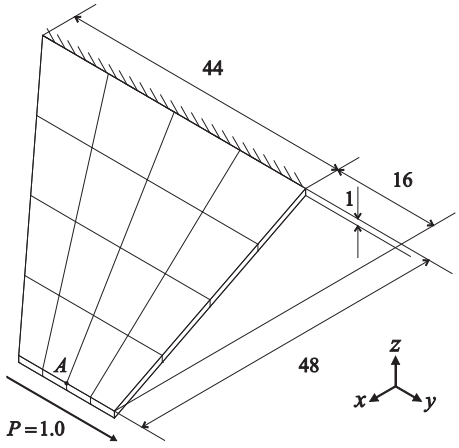

Fig. 7. Cook's problem (4×4 mesh, $E = 1.0$, plane stress conditions with $\nu = 1/3$; plane strain conditions with $\nu = 0.3$, 0.4 or 0.499).

Table 3
Predicted *y*-displacement at point A in Cook's problem with plane stress conditions.

Elements	Mesh				
	2×2	4×4	8×8	16×16	32×32
H8	10.9771	17.3332	21.5484	23.2055	23.7209
H8I9	20.3889	22.6184	23.4766	23.7740	23.8840
3D-MITC8	19.0821	22.2906	23.4092	23.7695	23.8893
Reference solution	23.9642				

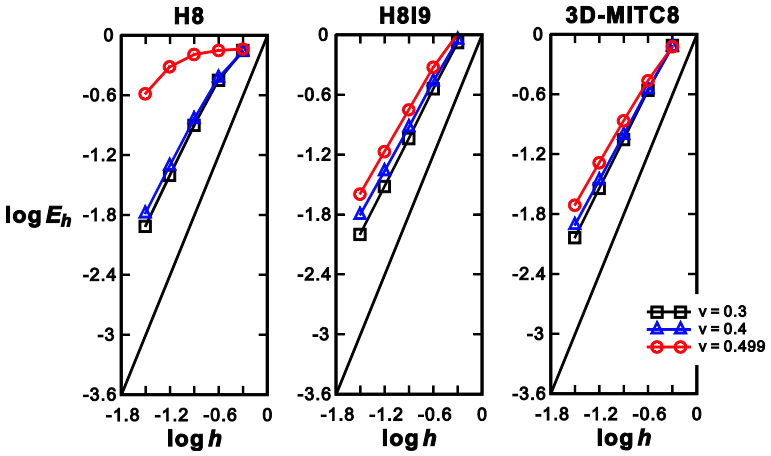

Fig. 8. Convergence curves for Cook's problem with plane strain conditions. The bold line represents the optimal convergence rate.

deformation, ${}^t_0c$ in Eq. (14) is zero, and thus the strain terms in Eq. (18b) are not activated.

We use as tying positions the Gauss numerical integration points $\left(\frac{1}{2}a = \frac{1}{\sqrt{3}}\right)$ for the in-plane bilinear interpolations of the normal and shear strains in Figs. 2 and 3 and the mid-points of the faces $\left(\frac{1}{2}a = 1\right)$ for the linear interpolations of the shear strains in Fig. 2. These positions of tying the normal and shear strains decrease the solution errors.

We employ the same assumed strain field for the incremental nonlinear strain ${}_0\widehat{\eta}_{ij}$, and hence the incremental strain components in the global Cartesian coordinate system are

$$ {}_0\overline{e}^{as}_{ij} = {}_0\tilde{e}_{kl}(\mathbf{i}_i \cdot {}^0\widehat{\mathbf{g}}^k)(\mathbf{i}_j \cdot {}^0\widehat{\mathbf{g}}^l),\ {}_0\overline{e}^{dil}_{ii} = {}_0\tilde{e}^{con}_{kl}(\mathbf{i}_i \cdot {}^0\widehat{\mathbf{g}}^k)(\mathbf{i}_i \cdot {}^0\widehat{\mathbf{g}}^l), $$

$$ \delta_0\overline{\eta}^{as}_{ij} = \delta_0\tilde{\eta}_{kl}(\mathbf{i}_i \cdot {}^0\widehat{\mathbf{g}}^k)(\mathbf{i}_j \cdot {}^0\widehat{\mathbf{g}}^l),\ \delta_0\overline{\eta}^{dil}_{ii} = \delta_0\tilde{\eta}^{con}_{kl}(\mathbf{i}_i \cdot {}^0\widehat{\mathbf{g}}^k)(\mathbf{i}_i \cdot {}^0\widehat{\mathbf{g}}^l), \tag{19} $$

in which superscripts '*as*' and '*dil*' denote assumed and dilatational strain parts. The dilatational strains are constructed only from the constant part of the assumed strains to alleviate volumetric locking.

The constant volumetric strain is obtained as [1,21]

$$ {}_0\overline{e}^{vol} = {}_0\overline{e}^{dil}_{xx} + {}_0\overline{e}^{dil}_{yy} + {}_0\overline{e}^{dil}_{zz} = \overline{\mathbf{B}}^{vol}\mathbf{u}_e, $$

$$ \delta_0\overline{\eta}^{vol} = \delta_0\overline{\eta}^{dil}_{xx} + \delta_0\overline{\eta}^{dil}_{yy} + \delta_0\overline{\eta}^{dil}_{zz} = \delta\mathbf{u}_e^T\overline{\mathbf{N}}^{vol}\mathbf{u}_e, \tag{20} $$

and the deviatoric strain components are obtained from

$$ {}_0\overline{e}^{dev}_{ij} = {}_0\overline{e}^{as}_{ij} - \frac{1}{3}{}_0\overline{e}^{vol}\delta_{ij} = \overline{\mathbf{B}}^{dev}_{ij}\mathbf{u}_e, $$

$$ \delta_0\overline{\eta}^{dev}_{ij} = \delta_0\overline{\eta}^{as}_{ij} - \frac{1}{3}\delta_0\overline{\eta}^{vol}\delta_{ij} = \delta\mathbf{u}_e^T\overline{\mathbf{N}}^{dev}_{ij}\mathbf{u}_e, \tag{21} $$

with the nodal displacement vector $\mathbf{u}_e = \begin{bmatrix}\mathbf{u}_1^T & \dots & \mathbf{u}_8^T\end{bmatrix}^T$. The efficient computation of the strain-displacement matrices given in Eqs. (20) and (21) is presented in Appendix B.

Table 4
CPU time used for evaluating the element stiffness matrices of Cook's problem (320 × 320 element mesh).

Elements	CPU time (s) used	Normalized CPU time
H8	16.1	1.0
H8I9	24.2	1.50
3D-MITC8	18.3	1.14
3D-MITC8/1	19.0	1.17
A laptop with dual core Intel 3.50 GHz CPU and 8.0 GB RAM is used		

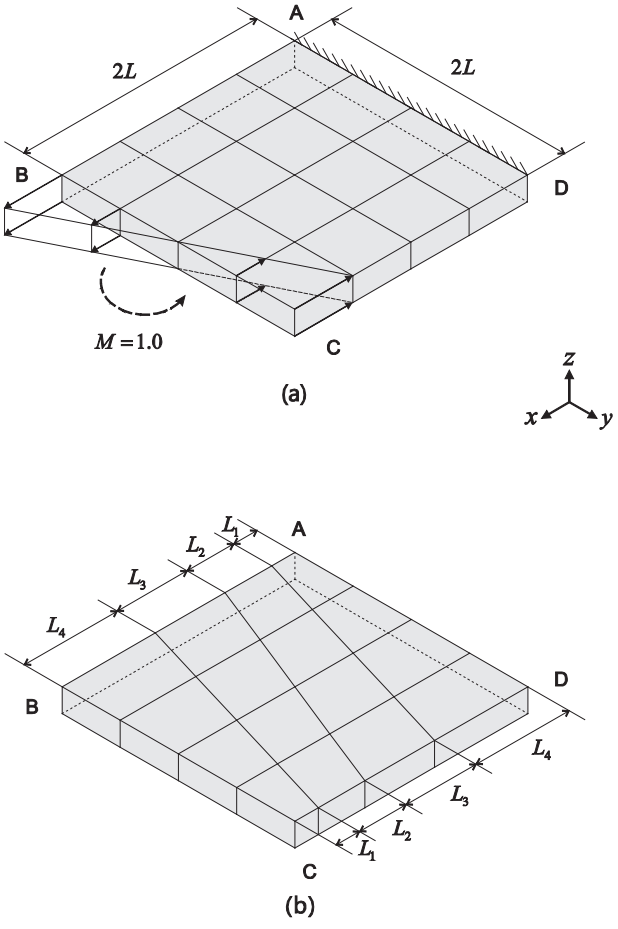

Fig. 9. Clamped square plate subjected to in-plane moment (plane strain conditions, $L = 1.0$, $E = 1.0$, $M = 1.0$, and $\nu = 0.3$, 0.4 or 0.499). (a) Problem description with regular mesh (4 × 4 mesh). (b) Distorted mesh (4 × 4 mesh).

The stiffness matrix ($^t\mathbf{K}$) and internal force vector ($^t_0\mathbf{F}$) are [1]

$$^t\mathbf{K} = \int_{^0V_e} \kappa \overline{\mathbf{B}}^{vol^T} \overline{\mathbf{B}}^{vol} d^0V_e + \int_{^0V_e} \overline{\mathbf{B}}_{ij}^{dev^T} C_{ij}^{dev} \overline{\mathbf{B}}_{ij}^{dev} d^0V_e + \int_{^0V_e} \frac{1}{3}(^t_0\overline{S}_{xx} + {}^t_0\overline{S}_{yy} + {}^t_0\overline{S}_{zz}) \overline{\mathbf{N}}^{vol} d^0V_e + \int_{^0V_e} {}^t_0\overline{S}_{ij} \overline{\mathbf{N}}_{ij}^{dev} d^0V_e,$$

$$^t_0\mathbf{F} = \int_{^0V_e} \overline{\mathbf{B}}^{vol^T} \frac{1}{3}\left(^t_0\overline{S}_{xx} + {}^t_0\overline{S}_{yy} + {}^t_0\overline{S}_{zz}\right) d^0V_e + \int_{^0V_e} \overline{\mathbf{B}}_{ij}^{dev^T} {}^t_0\overline{S}_{ij} d^0V_e, \quad (22)$$

in which $^t_0\overline{S}_{ij}$ denotes the second Piola-Kirchhoff stress measured in the global Cartesian coordinate system, and $\kappa = \frac{E}{3(1-2\nu)}$ is the bulk modulus with Young's modulus E and Poisson's ratio ν. For the linear isotropic material considered in this study, $C_{xx}^{dev} = C_{yy}^{dev} = C_{zz}^{dev} = \frac{E}{1+\nu}$ and $C_{xy}^{dev} = C_{yz}^{dev} = C_{zx}^{dev} = \frac{E}{2(1+\nu)}$.

The incremental Green-Lagrange strains in Eq. (10) are expressed using the linear and nonlinear strains in Eqs. (20) and (21), and the global incremental strain values are then obtained as

$${}_0\overline{\varepsilon}^{vol} = \overline{\mathbf{B}}^{vol}\mathbf{u}_e + \frac{1}{2}\mathbf{u}_e^T\overline{\mathbf{N}}^{vol}\mathbf{u}_e, \quad {}_0\overline{\varepsilon}_{ij}^{dev} = \overline{\mathbf{B}}_{ij}^{dev}\mathbf{u}_e + \frac{1}{2}\mathbf{u}_e^T\overline{\mathbf{N}}_{ij}^{dev}\mathbf{u}_e. \quad (23)$$

The second Piola-Kirchhoff stress is updated as

$$^{t+\Delta t}_0\overline{S}_{ij} = {}^t_0\overline{S}_{ij} + {}_0\overline{S}_{ij}, {}_0\overline{S}_{ij} = \kappa {}_0\overline{\varepsilon}^{vol}\delta_{ij} + C_{ij}^{dev} {}_0\overline{\varepsilon}_{ij}^{dev}, \quad (24)$$

and the nodal geometry is updated using Eq. (3).

Alternatively, we can construct an 8-node element using the assumed strain field in Eq. (18) to obtain a mixed displacement-pressure (u/p) formulation for alleviating volumetric locking.

The stiffness matrix ($^t\mathbf{K}$) and internal force vector ($^t_0\mathbf{F}$) of the 3D-MITC8/1 element are

$$^t\mathbf{K} = {}^t\mathbf{K}_{uu} - (1/K_{pp})\,{}^t\mathbf{K}_{up}\,{}^t\mathbf{K}_{up}^T,$$

$$^t\mathbf{K}_{uu} = \int_{^0V_e} \overline{\mathbf{B}}_{ij}^{dev^T} C_{ij}^{dev} \overline{\mathbf{B}}_{ij}^{dev} d^0V_e + \int_{^0V_e} \frac{1}{3}\left(^t_0\overline{S}_{xx} + {}^t_0\overline{S}_{yy} + {}^t_0\overline{S}_{zz}\right) \overline{\mathbf{N}}^{vol} d^0V_e + \int_{^0V_e} {}^t_0\overline{S}_{ij} \overline{\mathbf{N}}_{ij}^{dev} d^0V_e,$$

$$^t\mathbf{K}_{up} = -\int_{^0V_e} \overline{\mathbf{B}}^{vol^T} d^0V_e, \quad K_{pp} = -\int_{^0V_e} \frac{1}{\kappa} d^0V_e = -\frac{{}^0V}{\kappa},$$

$$^t_0\mathbf{F} = \int_{^0V_e} \overline{\mathbf{B}}^{vol^T} \frac{1}{3}\left(^t_0\overline{S}_{xx} + {}^t_0\overline{S}_{yy} + {}^t_0\overline{S}_{zz}\right) d^0V_e + \int_{^0V_e} \overline{\mathbf{B}}_{ij}^{dev^T} {}^t_0\overline{S}_{ij} d^0V_e. \quad (25)$$

The single pressure variable (p_e) is

$$p_e = -(1/K_{pp})\mathbf{K}_{up}^T\mathbf{u}_e, \quad (26)$$

and the second Piola-Kirchhoff stress is updated as

$$^{t+\Delta t}_0\overline{S}_{ij} = {}^t_0\overline{S}_{ij} + {}_0\overline{S}_{ij}, {}_0\overline{S}_{ij} = -p_e\delta_{ij} + C_{ij}^{dev} {}_0\overline{\varepsilon}_{ij}^{dev}. \quad (27)$$

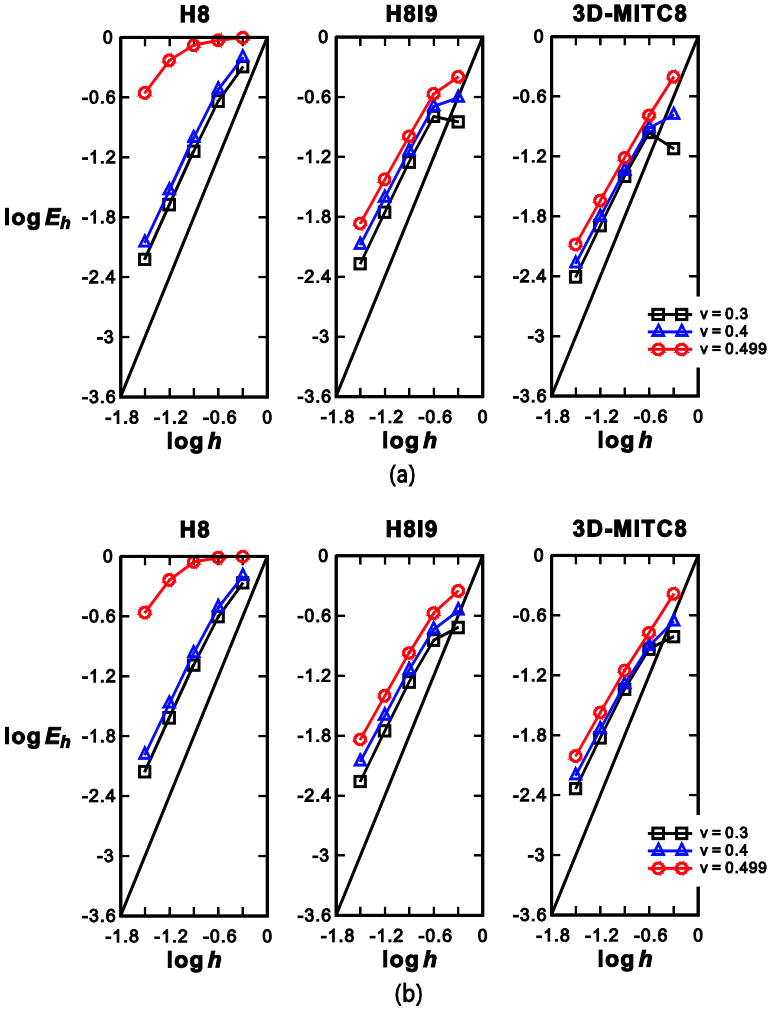

Fig. 10. Convergence curves for the clamped square plate subjected to in-plane moment using (a) uniform meshes and (b) distorted meshes. The bold line represents the optimal convergence rate.

When compared with the 3D-MITC8 element, the 3D-MITC8/1 element shows the same performance in linear analyses and can give slightly different solutions in nonlinear analyses. For the numerical solutions below, the results are the same as for the 3D-MITC8 element unless otherwise noted.

In the finite element solutions, we use $2 \times 2 \times 2$ Gauss integration over the element volume considered.

4. Illustrative solutions

In this section, we present the performance of the new 3D solid element through the solutions of various 3D examples. Comparisons are made with the standard displacement based 8-node element referred to as "H8" as well as the standard 8-node incompatible modes element referred to as "H8I9", see Refs. [1,3–5].

First, the new 3D solid element is assessed considering the basic numerical tests. Then the performance of the new 3D solid element is investigated in linear plane stress and plane strain analyses, namely, a cantilever beam problem, Cook's problem, a clamped square plate problem, a pressurized cavity problem, and a clamped plate subjected to a uniform pressure. The geometric nonlinear solutions are included to test the occurrence of instability: a cantilever subjected to tip forces, a rubber block problem, and a panel problem. We use ADINA to obtain the solutions of the geometric nonlinear problems with the incompatible modes element [22]. In all analyses we assume that the material response is described by Young's modulus E and Poisson's ratio ν, where we recognize that there is a strain limit that such material can be subjected to before a material model instability occurs [1].

Using the derivations in Appendix B, we have found that the calculation of the 3D-MITC8 element stiffness matrix is not much more expensive than the calculation of the H8 element stiffness matrix commonly used (see Section 4.3 for an example).

4.1. Basic numerical tests

We consider the isotropy, zero energy mode and patch tests in linear analysis.

The spatially isotropic behavior and invariance to the nodal numbering is important for any element [1,17,19]. The 3D-MITC8 element passes the isotropy test.

In the spurious zero energy mode test, the stiffness matrix of a single unsupported element should show only zero eigenvalues corresponding to the correct rigid body modes. Six rigid body modes corresponding to the 3 translations and 3 rotations should be present. The 3D-MITC8 element passes this test.

In the patch tests [1,15,23], the patch of elements shown in Fig. 5 is subjected to the minimum number of constraints to prevent rigid body motions, and forces are applied at the boundary corresponding to the constant stress states. The predicted normal and shearing stresses should be the analytically correct values at any location within the patch of elements. The 3D-MITC8 element passes the patch tests.

4.2. Cantilever problem

We solve the cantilever problem shown in Fig. 6. The structure is subjected to a shearing force at its tip. The cantilever is modeled using regular and distorted meshes with four elements as in Refs. [20,24,25].

Tables 1 and 2 give the tip vertical displacement at point A and the xx-component of stress at point B with reference to the reference solutions. As when using the H8I9 element, the use of the 3D-MITC8 element gives the exact solution with a regular mesh. For the distorted mesh case, the solution using the 3D-MITC8 element is much more accurate than when using the H8 element, and not much less accurate than obtained using the H8I9 element.

4.3. Cook's cantilever problem

We consider Cook's problem shown in Fig. 7 [4,20,24,26]. The cantilever is clamped at one end and is subjected to a distributed shearing force of total magnitude P at its tip. We consider the solutions using plane stress conditions with Poisson's ratio $\nu = 1/3$, plane strain conditions with $\nu = 0.3$, 0.4 and 0.499, and meshes of $N \times N$ elements with $N = 2, 4, 8, 16$ and 32. The plane strain condition is modeled by imposing $w = 0$ for the entire mesh.

Table 3 gives the vertical displacement at point A for the plane stress case. The performance of the 3D-MITC8 element is similar to that of the H8I9 element. For the plane strain case, we measure the solution error using the s-norm [27,28] with reference solutions obtained using a 72×72 mesh of the standard 27-node displacement-based element for the cases $\nu = 0.3$, 0.4 and the 27/4 element for the case $\nu = 0.499$ [1].

The s-norm used is given by

$$\|\mathbf{u}_{ref} - \mathbf{u}_h\|_s^2 = \int_{\Omega_{ref}} \Delta\boldsymbol{\varepsilon}^T \Delta\boldsymbol{\tau} d\Omega_{ref}, \quad \text{with } \Delta\boldsymbol{\varepsilon} = \boldsymbol{\varepsilon}_{ref} - \boldsymbol{\varepsilon}_h, \quad \Delta\boldsymbol{\tau} = \boldsymbol{\tau}_{ref} - \boldsymbol{\tau}_h, \tag{28}$$

and then the relative error is

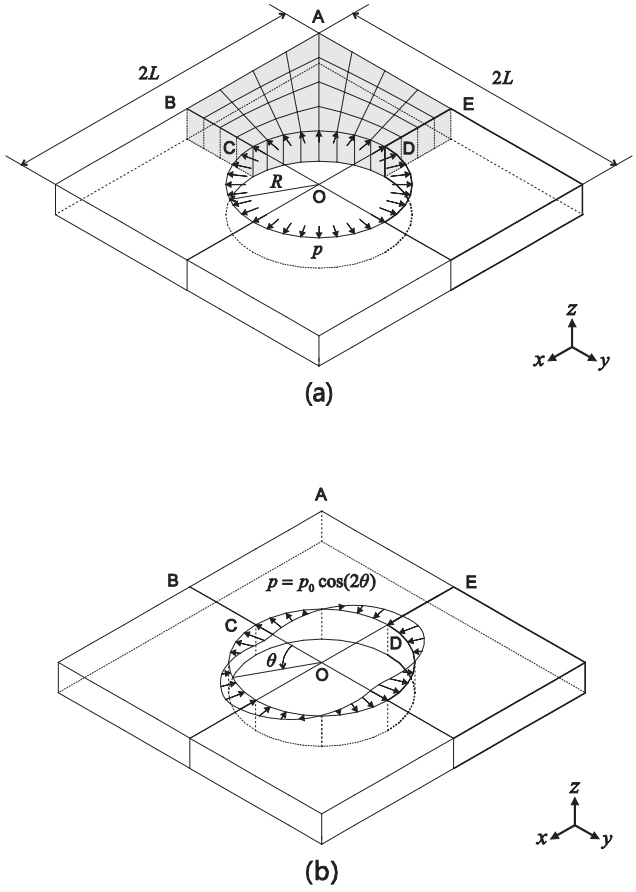

Fig. 11. Pressurized cavity problem (plane strain conditions, $L = 1.0$, $E = 1.0$, $p = 1.0$ for uniform and $p_0 = 1.0$ for smoothly varying loads, and $\nu = 0.3$, 0.4 or 0.499). (a) Problem description with uniform pressure (4×8 mesh). (b) Smoothly varying pressure.

$$E_h = \frac{\|\mathbf{u}_{ref} - \mathbf{u}_h\|_s^2}{\|\mathbf{u}_{ref}\|_s^2}, \tag{29}$$

where $\mathbf{u}_{ref}$ is the reference solution, $\mathbf{u}_h$ is the solution of the finite element discretization, the subscript h corresponds to the element size used, $\boldsymbol{\varepsilon}$ and $\boldsymbol{\tau}$ are the strain and stress vectors, and E_h is the relative error.

The behavior of an element is optimal if the convergence for the element in a sequence of meshes is given by

$$E_h \cong Ch^2, \tag{30}$$

in which C is a constant independent of the material properties and h is the element size.

Fig. 8 shows the convergence of the relative error as a function of the element size $h = 1/N$. For $\nu = 0.499$, the convergence is severely degraded when using the H8 element. The 3D-MITC8 and H8I9 elements behave nearly optimally and show comparable performance.

To indicate the computational effectiveness of the new element, Table 4 gives the CPU time used to calculate the element stiffness matrices for a fine mesh with $N = 320$, that is, 102,400 elements. We employ the standard formulations for the H8 and H8I9 elements, with the internal degrees of freedom of the H8I9 element condensed out [1,3–5]. The time used for the 3D-MITC8 element is larger than for the standard H8 element, but not by much.

4.4. Clamped square plate subjected to an in-plane moment

We solve the clamped square plate problem shown in Fig. 9 [20] and assume plane strain conditions with Poisson's ratios $\nu = 0.3$, 0.4 and 0.499. For the solutions, we use regular and distorted meshes with $N \times N$ elements and $N = 2$, 4, 8, 16 and 32, see Fig. 9(a) and (b), where the element edges are discretized in the ratio $L_1{:}L_2{:}L_3{:}\ldots{:}L_N = 1{:}2{:}3{:}\ldots{:}N$. The following boundary conditions are imposed: $u = v = w = 0$ along AD, and $w = 0$ for the entire mesh.

The relative error is measured using the s-norm with the reference solutions obtained using a 72×72 mesh of the standard 27-node displacement-based element for the cases $\nu = 0.3$, 0.4 and the 27/4 element for the case $\nu = 0.499$. Fig. 10 shows a comparable performance of the 3D-MITC8 and H8I9 elements, where the convergence is nearly optimal for the uniform and distorted meshes.

4.5. Pressurized cavity problem

We consider a square structural domain with an internally pressurized circular cavity as shown in Fig. 11. Plane strain conditions are assumed with Poisson's ratios $\nu = 0.3$, 0.4 and 0.499. Because of symmetry, only one-quarter of the structure is modeled using $N \times 2N$ elements with $N = 2$, 4, 8, 16 and 32. The following bound-

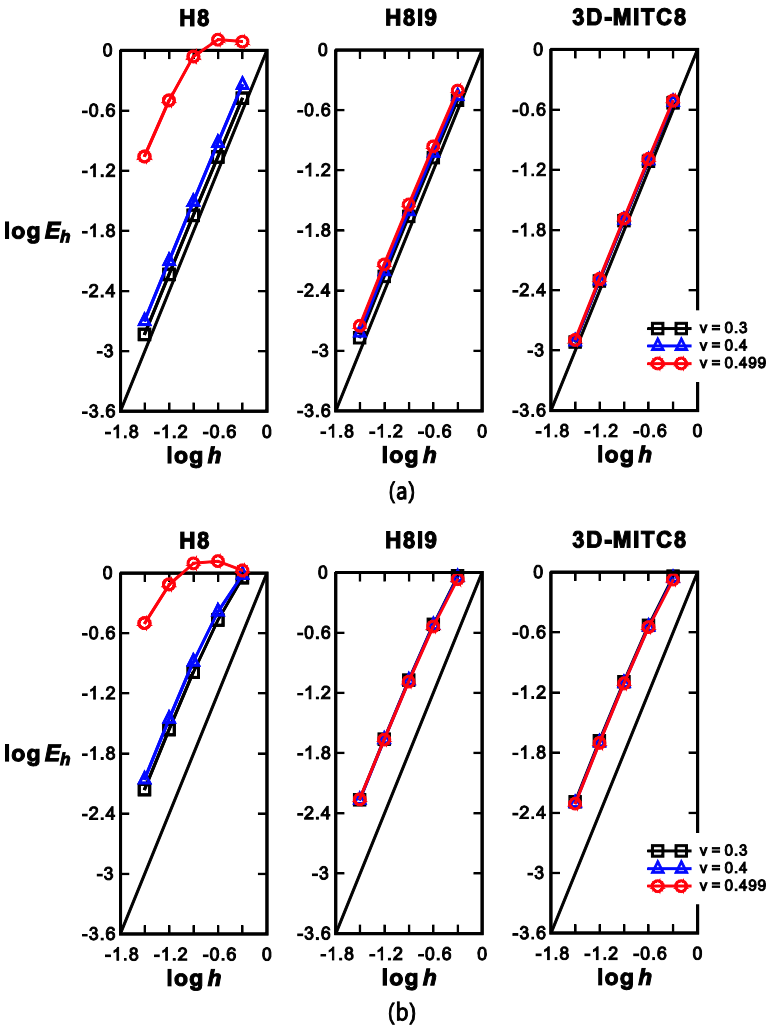

Fig. 12. Convergence curves for the pressurized cavity problem using (a) the uniform and (b) smoothly varying loads. The bold line represents the optimal convergence rate.

ary conditions are imposed: $u = 0$ along BC, $v = 0$ along DE, and $w = 0$ for the entire mesh.

The structure undergoes in-plane compression or bending according to the type of internal pressure p used. We test the cases of uniform internal pressure, see Fig. 11(a), and smoothly varying pressure, see Fig. 11(b).

Fig. 12 shows the convergence of the solutions measured using the s-norm, for which the reference solution is obtained with a 36 $\times$ 72 mesh of the standard 27-node displacement-based element for the cases $\nu = 0.3$, 0.4 and the 27/4 element for the case $\nu = 0.499$. Unlike the H8 element which severely locks near the incompressible limit, the 3D-MITC8 and H8I9 elements behave optimally.

4.6. Clamped square plate subjected to a uniform pressure

We consider a clamped square plate transversely loaded by a uniform pressure, see Fig. 13(a) [17,19,20]. Utilizing symmetry, only one quarter of the plate is modeled using $N \times N$ elements with $N = 4$, 8, 16, 32 and 64. We vary the ratio of the shell thickness to the overall dimension of the structure, $t/L = 1/10$, 1/100 and 1/1000. The element size is $h = L/N$. The boundary conditions are $u = \theta_y = 0$ along BC, $v = \theta_x = 0$ along DC and $u = v = w = \theta_x = \theta_y = 0$ along AB and AD. We use only one layer of elements in the thickness direction.

We also perform the convergence studies with the distorted mesh pattern shown in Fig. 13(b), where each edge is discretized by the elements in the following ratio: $L_1{:}L_2{:}L_3{:}\ldots{:}L_N$ = 1:2:3:...:N for the $N \times N$ element mesh.

Fig. 14 shows the convergence measured using the s-norm; the reference solution is obtained using a 72 $\times$ 72 element mesh of the MITC9 shell element [28,29]. The element behavior is optimal if the convergence curves have the optimal slope and the curves are independent of the plate thickness and material properties. For the 3D solid elements, we can hardly expect to see as good a performance as when using shell or plate elements. However, the 3D-MITC8 element shows the optimal convergence behavior when using the regular mesh. The convergence behavior deteriorates when a distorted mesh is used, but the performance of the 3D-MITC8 element is better than the performance of the H8I9 element.

4.7. Cantilever in large displacements

We solve the cantilever problem shown in Fig. 15; the structure is subjected to tip forces of magnitude F. To test the mixed effect of compression and bending, two tip forces are applied at corners of the structure. The increment in load per step is 2.0. The fully clamped boundary condition of $u = v = w = 0$ is applied at the bottom.

Figs. 16 and 17 present the load-displacement curves and the deformed shapes, respectively. The reference solution is obtained using the standard 27-node displacement-based element. The 3D-MITC8 and incompatible modes elements follow the reference behavior, however, using the H8I9 element, the cantilever is predicted to already collapse at $F = 68.0$ due to the propagation of an element instability near the bottom of the model.

4.8. Rubber blocks in large displacements and large strains

We solve the rubber block problems shown in Fig. 18 [12,13,20]. The structures are supported at the bottom, loaded with the pressure p in plane strain conditions with $\nu = 0.49$. The increment in load per step is 1.2.

We analyze the rectangular and trapezoidal structures using coarse meshes and, of course, do not claim to have reached solution convergence of the continuum problems. The purpose of the solutions is to investigate whether an instability arises when using the 3D-MITC8 element.

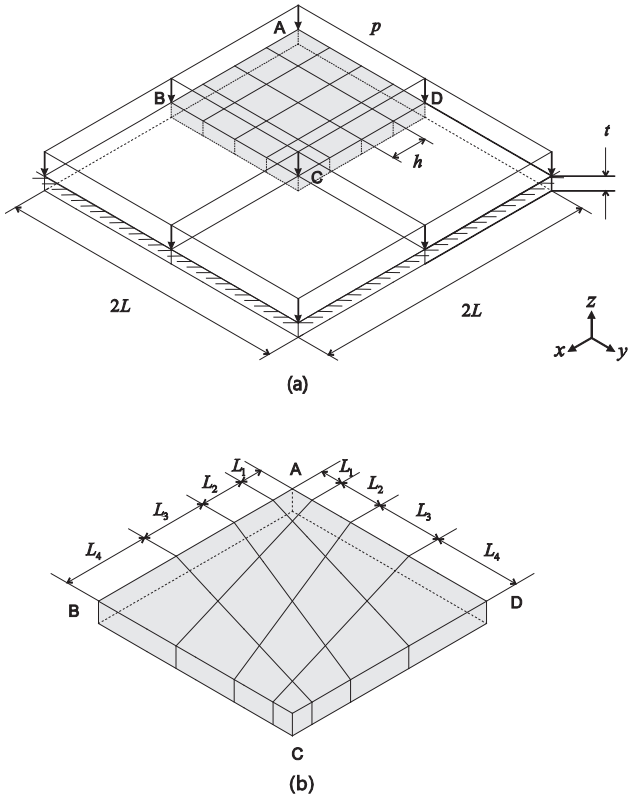

Fig. 13. Clamped square plate with uniform pressure ($L = 1.0$, $E = 1.7472 \times 10^7$, $p = 1.0$ and $\nu = 0.3$). (a) Problem description with regular mesh (4 $\times$ 4 mesh). (b) Distorted mesh (4 $\times$ 4 mesh).

Fig. 19 shows the calculated load-displacement curves. Since Poisson's ratio is not very close to 0.5, we obtain the reference solutions using the standard 27-node displacement-based element. The standard H8 element shows a too stiff behavior. Using the H8I9 element, the analysis stops at the spurious collapse loads $p = 80.4$ and $p = 85.2$ for the rectangular and trapezoidal structures, respectively. The solutions using the 3D-MITC8 element are as stable as when using the 2D-MITC4/1 or the standard 27-node elements. Fig. 20 shows deformed shapes obtained using the 3D-MITC8 element; these shapes are acceptable in contrast to those obtained when using the H8I9 element which show spurious hour-glass patterns.

4.9. Rubber panel in large displacements and large strains

We consider the panel shown in Fig. 21. The pressure load p is applied asymmetrically on the top in order to also have significant bending of the structure. The increment in load per step is 1.6. Since the mesh is coarse, we do not claim to have reached convergence in the solution of the continuum problem. The purpose of this problem is to investigate whether a spurious instability arises.

Fig. 22 shows the load-displacement curves. The reference solution is obtained using the standard 27-node displacement-based element. While the analysis using the H8I9 element predicts a spurious path of solution, the prediction using the 3D-MITC8 element closely follows the reference load-displacement curve. The deformed shapes are compared in Fig. 23. Unlike the H8I9 element

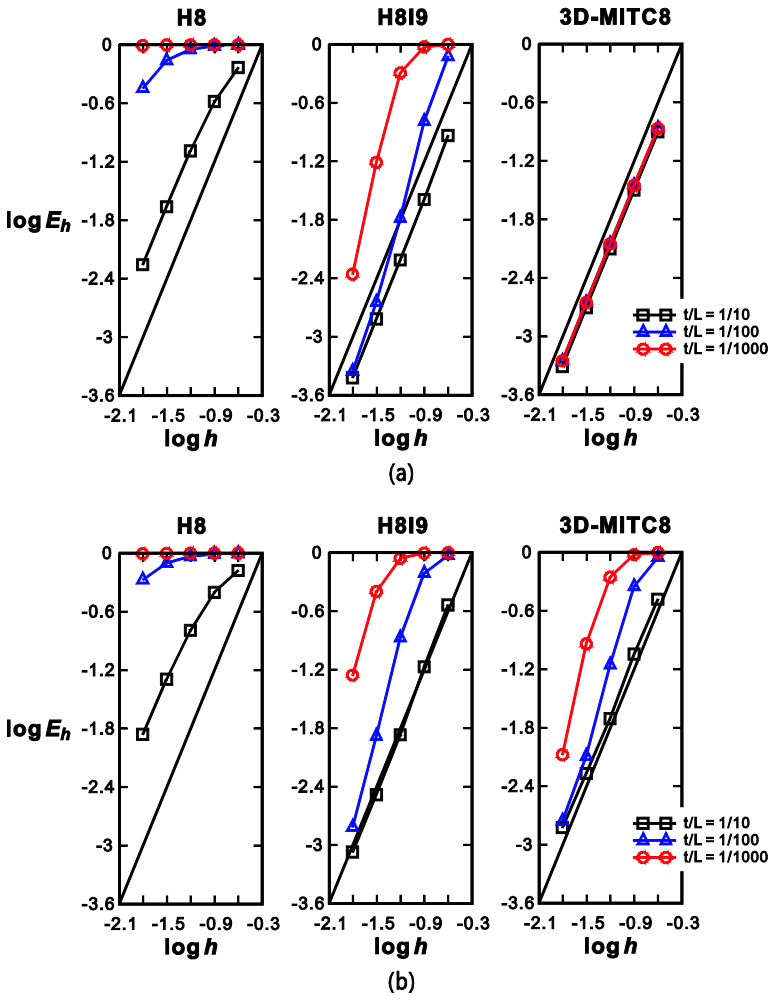

Fig. 14. Convergence curves for the clamped square plate problem using (a) regular and (b) distorted meshes. The bold line represents the optimal convergence rate.

mesh which shows strong hour-glass shapes, the 3D-MITC8 element mesh deforms smoothly as in the reference solution.

5. Concluding remarks

We proposed a new 3D 8-node solid element based on the MITC approach for linear and nonlinear analyses. We established the assumed strain field from physical considerations using a truss structure to idealize the solid element and previously obtained knowledge regarding MITC element formulations, specifically the 2D-MITC4, the 2D-MITC4/1 and the MITC4 shell elements [15,20]. However, unlike in previous MITC element formulations, we needed to include stabilization terms of displacement-based shear strains to suppress spurious modes in geometrically nonlinear solutions. These stabilization strain terms are only, and then automatically, activated in geometrically nonlinear analyses when needed.

The new 3D-MITC8 passes all basic element tests and we presented various problem solutions to illustrate the predictive capabilities of the element. In linear analyses, the element compares well in the accuracy of solutions reached with the H8I9 element but is computationally more efficient because no incompatible modes are used. In geometrically nonlinear analyses, the element did not show instabilities as observed when using the H8I9 element. However, it would be valuable to further study the element and in particular to obtain deeper insight into the element formulation through a mathematical analysis.

Appendix A. Representation of assumed strain field using characteristic vectors

Here we decompose the covariant strain components using the characteristic vectors and use the decomposition to represent the constant assumed strain in Eq. (18).

Note that the incremental linear and nonlinear strain parts in Eq. (11) can be expressed as

$$
\begin{aligned}
{}_0e_{ij}(r,s,t) &= ({}^tx_I u_J + {}^ty_I v_J + {}^tz_I w_J) n_{ijIJ}(r,s,t),\\
{}_0\eta_{ij}(r,s,t) &= (u_I u_J + v_I v_J + w_I w_J) n_{ijIJ}(r,s,t),
\end{aligned}
\tag{A.1}
$$

in which $I, J = 1,\ldots,8$ are node numbers. Note that any part of incremental strains can be expressed using the corresponding nodal constants (n_{ijIJ} with $n_{ijIJ} = n_{jiIJ} = n_{ijJI} = n_{jiJI}$). The geometry is described and corresponding incremental displacements are

$$
\begin{aligned}
{}^t\mathbf{X}^C &= \left[{}^t\mathbf{x}^{[1]} \quad {}^t\mathbf{x}^{[2]} \quad {}^t\mathbf{x}^{[3]} \quad {}^t\mathbf{x}^{[4]} \quad {}^t\mathbf{x}^{[5]} \quad {}^t\mathbf{x}^{[6]} \quad {}^t\mathbf{x}^{[7]} \right]\\
&= \left[{}^t\widehat{\mathbf{g}}_r \quad {}^t\widehat{\mathbf{g}}_s \quad {}^t\widehat{\mathbf{g}}_t \quad {}^t\mathbf{x}_{rs} \quad {}^t\mathbf{x}_{st} \quad {}^t\mathbf{x}_{tr} \quad {}^t\mathbf{x}_{rst} \right],
\end{aligned}
$$

$$
\mathbf{U}^C = {}^{t+\Delta t}\mathbf{X}^C - {}^t\mathbf{X}^C = \left[\mathbf{u}^{[1]} \quad \mathbf{u}^{[2]} \quad \mathbf{u}^{[3]} \quad \mathbf{u}^{[4]} \quad \mathbf{u}^{[5]} \quad \mathbf{u}^{[6]} \quad \mathbf{u}^{[7]} \right],
$$

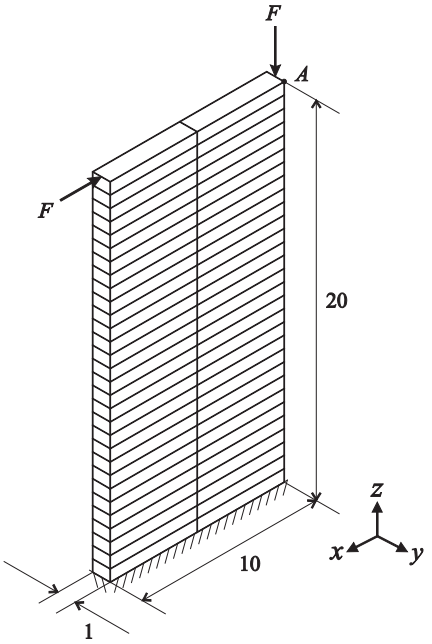

Fig. 15. Cantilever subjected to tip forces ($2 \times 1 \times 30$ mesh, $E = 1.0 \times 10^3$ and $\nu = 0.0$).

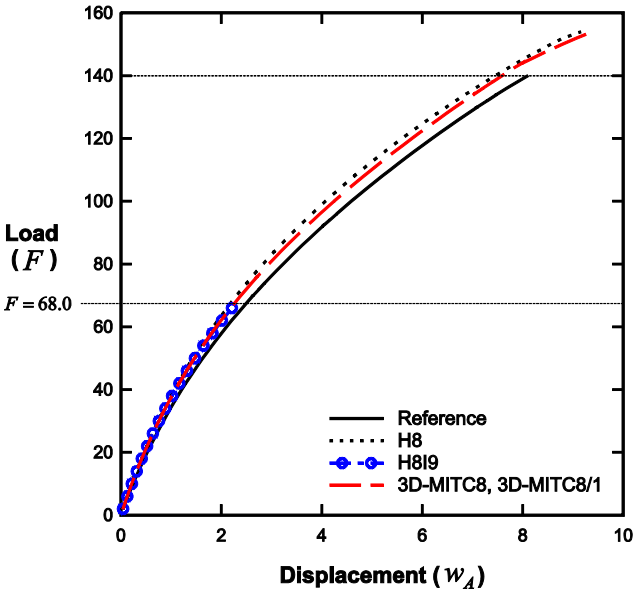

Fig. 16. Load-displacement curves for the cantilever.

$$\mathbf{u}^{[K]} = \begin{bmatrix} u^{[K]} & v^{[K]} & w^{[K]} \end{bmatrix}^T \quad \text{with } K = 1, \ldots, 7. \tag{A.2}$$

Using Eq. (A.2), we define following representative incremental strains ($e^{[K|L]}$ and $\eta^{[K|L]}$) and the corresponding nodal constants ($n_{IJ}^{[K|L]}$),

$$e^{[K|L]} = \frac{1}{2}\left({}^t\mathbf{x}^{[K]} \cdot \mathbf{u}^{[L]} + \mathbf{u}^{[K]} \cdot {}^t\mathbf{x}^{[L]}\right) = \left({}^tx_I u_J + {}^ty_I v_J + {}^tz_I w_J\right) n_{IJ}^{[K|L]},$$

$$\eta^{[K|L]} = \frac{1}{2}\left(\mathbf{u}^{[K]} \cdot \mathbf{u}^{[L]} + \mathbf{u}^{[K]} \cdot \mathbf{u}^{[L]}\right) = \left(u_I u_J + v_I v_J + w_I w_J\right) n_{IJ}^{[K|L]},$$

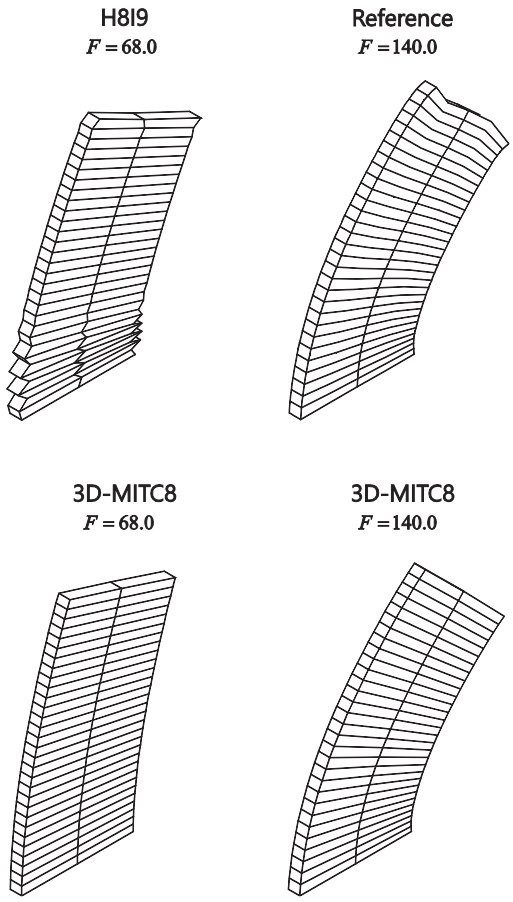

Fig. 17. Deformed shapes for the cantilever.

$$n_{IJ}^{[K|L]} = \frac{1}{128}\left(\varsigma_I^{[K]}\varsigma_J^{[L]} + \varsigma_J^{[K]}\varsigma_I^{[L]}\right) \quad \text{with } I, J = 1, \ldots, 8 \text{ and } K, L = 1, \ldots, 7,$$

$$\begin{bmatrix} \varsigma_I^{[1]} & \varsigma_I^{[2]} & \varsigma_I^{[3]} & \varsigma_I^{[4]} & \varsigma_I^{[5]} & \varsigma_I^{[6]} & \varsigma_I^{[7]} \end{bmatrix} = \begin{bmatrix} \xi_I & \eta_I & \zeta_I & \xi_I\eta_I & \eta_I\zeta_I & \zeta_I\xi_I & \xi_I\eta_I\zeta_I \end{bmatrix}. \tag{A.3}$$

Using Eq. (A.2) in Eq. (4),

$${}^t\mathbf{g}_r = \frac{\partial\, {}^t\mathbf{x}}{\partial r} = {}^t\mathbf{x}^{[1]} + s\,{}^t\mathbf{x}^{[4]} + t\,{}^t\mathbf{x}^{[6]} + st\,{}^t\mathbf{x}^{[7]},$$
$$\mathbf{u}_{,r} = \frac{\partial \mathbf{u}}{\partial r} = \mathbf{u}^{[1]} + s\mathbf{u}^{[4]} + t\mathbf{u}^{[6]} + st\mathbf{u}^{[7]},$$

$${}^t\mathbf{g}_s = \frac{\partial\, {}^t\mathbf{x}}{\partial s} = {}^t\mathbf{x}^{[2]} + t\,{}^t\mathbf{x}^{[5]} + r\,{}^t\mathbf{x}^{[4]} + tr\,{}^t\mathbf{x}^{[7]},$$
$$\mathbf{u}_{,s} = \frac{\partial \mathbf{u}}{\partial s} = \mathbf{u}^{[2]} + t\mathbf{u}^{[5]} + r\mathbf{u}^{[4]} + tr\mathbf{u}^{[7]},$$

$${}^t\mathbf{g}_t = \frac{\partial\, {}^t\mathbf{x}}{\partial t} = {}^t\mathbf{x}^{[3]} + r\,{}^t\mathbf{x}^{[6]} + s\,{}^t\mathbf{x}^{[5]} + rs\,{}^t\mathbf{x}^{[7]},$$
$$\mathbf{u}_{,t} = \frac{\partial \mathbf{u}}{\partial t} = \mathbf{u}^{[3]} + r\mathbf{u}^{[6]} + s\mathbf{u}^{[5]} + rs\mathbf{u}^{[7]}. \tag{A.4}$$

Using Eqs. (A.1), (A.3) and (A.4) with Eq. (11) we obtain the nodal constants for the covariant strain

$$n_{rrIJ}(r,s,t) = n_{IJ}^{[1|1]} + 2sn_{IJ}^{[1|4]} + 2tn_{IJ}^{[1|6]} + 2st(n_{IJ}^{[1|7]} + n_{IJ}^{[4|6]}) + s^2 n_{IJ}^{[4|4]} + 2s^2 t n_{IJ}^{[4|7]} + t^2 n_{IJ}^{[6|6]} + 2st^2 n_{IJ}^{[6|7]} + s^2 t^2 n_{IJ}^{[7|7]},$$

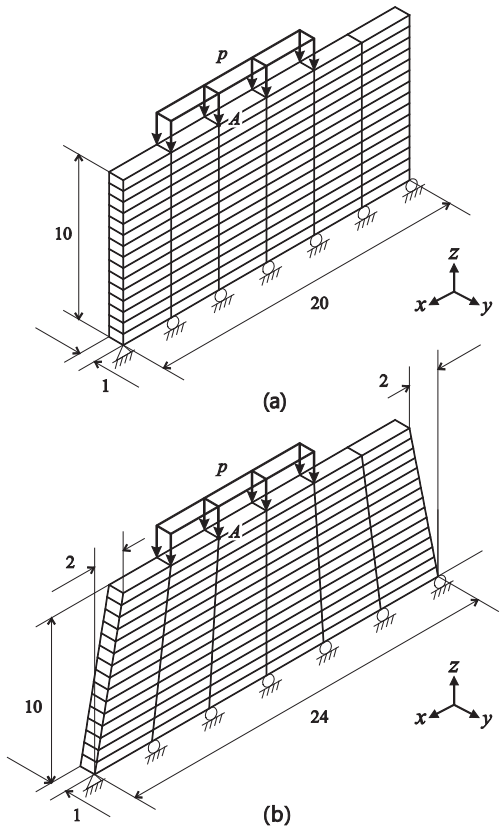

Fig. 18. Rubber blocks subjected to pressure ($6 \times 1 \times 15$ mesh, $E = 1.0 \times 10^3$ and $\nu = 0.49$). (a) Rectangular block. (b) Trapezoidal block.

$$n_{ssIJ}(r,s,t) = n_{IJ}^{[2|2]} + 2tn_{IJ}^{[2|5]} + 2rn_{IJ}^{[2|4]} + 2tr(n_{IJ}^{[2|7]} + n_{IJ}^{[4|5]}) + t^2 n_{IJ}^{[5|5]} + 2t^2 rn_{IJ}^{[5|7]} + r^2 n_{IJ}^{[4|4]} + 2tr^2 n_{IJ}^{[4|7]} + t^2 r^2 n_{IJ}^{[7|7]},$$

$$n_{ttIJ}(r,s,t) = n_{IJ}^{[3|3]} + 2rn_{IJ}^{[3|6]} + 2sn_{IJ}^{[3|5]} + 2rs(n_{IJ}^{[3|7]} + n_{IJ}^{[5|6]}) + r^2 n_{IJ}^{[6|6]} + 2r^2 sn_{IJ}^{[6|7]} + s^2 n_{IJ}^{[5|5]} + 2rs^2 n_{IJ}^{[5|7]} + r^2 s^2 n_{IJ}^{[7|7]},$$

$$n_{rsIJ}(r,s,t) = n_{IJ}^{[1|2]} + t(n_{IJ}^{[1|5]} + n_{IJ}^{[2|6]}) + rn_{IJ}^{[1|4]} + tr(n_{IJ}^{[4|6]} + n_{IJ}^{[1|7]}) + sn_{IJ}^{[2|4]} + st(n_{IJ}^{[4|5]} + n_{IJ}^{[2|7]}) + rsn_{IJ}^{[4|4]} + 2rstn_{IJ}^{[4|7]} + t^2 n_{IJ}^{[5|6]} + t^2 rn_{IJ}^{[6|7]} + st^2 n_{IJ}^{[5|7]} + rst^2 n_{IJ}^{[7|7]},$$

$$n_{stIJ}(r,s,t) = n_{IJ}^{[2|3]} + r(n_{IJ}^{[2|6]} + n_{IJ}^{[3|4]}) + sn_{IJ}^{[2|5]} + rs(n_{IJ}^{[4|5]} + n_{IJ}^{[2|7]}) + tn_{IJ}^{[3|5]} + tr(n_{IJ}^{[5|6]} + n_{IJ}^{[3|7]}) + stn_{IJ}^{[5|5]} + 2rstn_{IJ}^{[5|7]} + r^2 n_{IJ}^{[4|6]} + r^2 sn_{IJ}^{[4|7]} + tr^2 n_{IJ}^{[6|7]} + r^2 stn_{IJ}^{[7|7]},$$

$$n_{trIJ}(r,s,t) = n_{IJ}^{[1|3]} + s(n_{IJ}^{[3|4]} + n_{IJ}^{[1|5]}) + tn_{IJ}^{[3|6]} + st(n_{IJ}^{[5|6]} + n_{IJ}^{[3|7]}) + rn_{IJ}^{[1|6]} + rs(n_{IJ}^{[4|6]} + n_{IJ}^{[1|7]}) + trn_{IJ}^{[6|6]} + 2rstn_{IJ}^{[6|7]} + s^2 n_{IJ}^{[4|5]} + s^2 tn_{IJ}^{[5|7]} + rs^2 n_{IJ}^{[4|7]} + rs^2 tn_{IJ}^{[7|7]}, \quad \text{(A.5)}$$

with $n_{rrIJ} = n_{11IJ}$, $n_{ssIJ} = n_{22IJ}$, $n_{ttIJ} = n_{33IJ}$, $n_{rsIJ} = n_{12IJ}$, $n_{stIJ} = n_{23IJ}$ and $n_{trIJ} = n_{31IJ}$. Using Eq. (17) with Eq. (A.3),

$$\tilde{n}_{IJ}^{[K|7]} = {}^t d_r n_{IJ}^{[K|1]} + {}^t d_s n_{IJ}^{[K|2]} + {}^t d_t n_{IJ}^{[K|3]} \quad \text{with } K = 1,\ldots,6,$$

$$\tilde{n}_{IJ}^{[7|7]} = {}^t d_r^2 n_{IJ}^{[1|1]} + {}^t d_s^2 n_{IJ}^{[2|2]} + {}^t d_t^2 n_{IJ}^{[3|3]} + 2{}^t d_r {}^t d_s n_{IJ}^{[1|2]} + 2{}^t d_s {}^t d_t n_{IJ}^{[2|3]} + 2{}^t d_t {}^t d_r n_{IJ}^{[1|3]}. \quad \text{(A.6)}$$

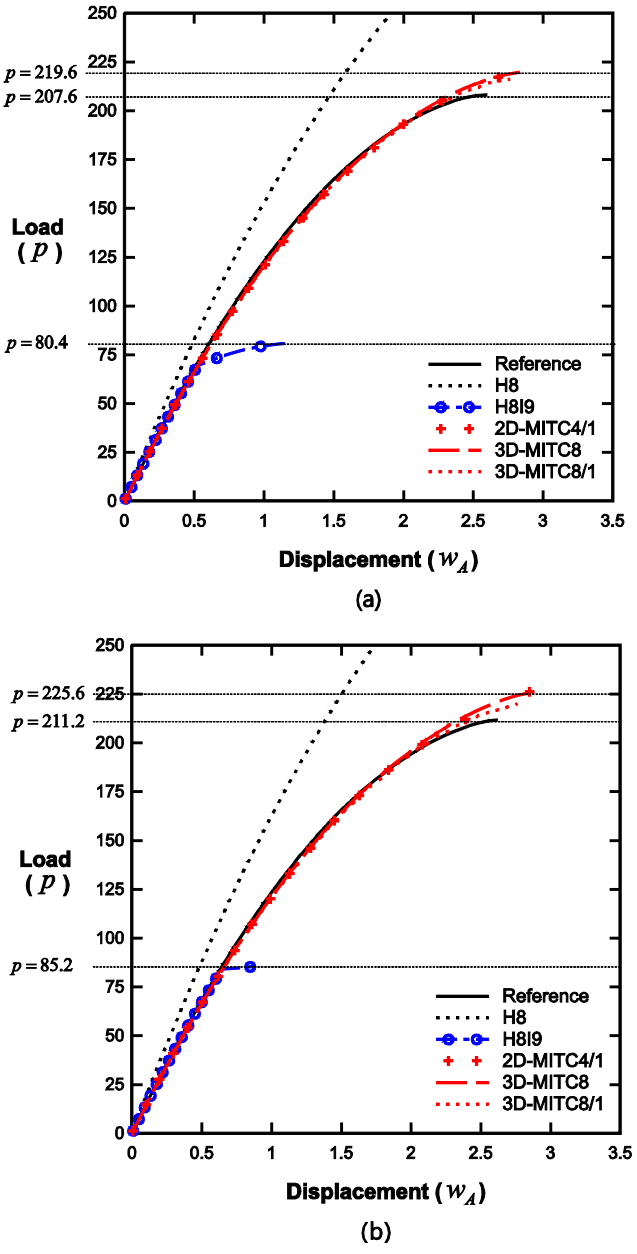

Fig. 19. Load-displacement curves for the rubber blocks. (a) Rectangular block. (b) Trapezoidal block.

Substituting $\tilde{n}_{IJ}^{[K|7]}$ for $n_{IJ}^{[K|7]}$ ($K = 1,\ldots,7$) in Eq. (A.5), we obtain the nodal constants for the assumed covariant strain $\tilde{\mathbf{n}}_{IJ}(r,s,t) = \left[\tilde{n}_{11IJ} \quad \tilde{n}_{22IJ} \quad \tilde{n}_{33IJ} \quad \tilde{n}_{12IJ} \quad \tilde{n}_{23IJ} \quad \tilde{n}_{31IJ}\right]$.

Appendix B. Calculation of strain-displacement matrices

We aim to obtain good computational efficiency in the evaluation of the element matrices.

Rearranging the strain transformation in Eq. (12),

$$\widehat{\mathbf{n}}_{IJ}(r,s,t)^T = \widehat{\mathbf{G}}\,\mathbf{n}_{IJ}(r,s,t)^T,$$

$$\widehat{\mathbf{n}}_{IJ}(r,s,t) = \left[\widehat{n}_{11IJ} \quad \widehat{n}_{22IJ} \quad \widehat{n}_{33IJ} \quad \widehat{n}_{12IJ} \quad \widehat{n}_{23IJ} \quad \widehat{n}_{31IJ}\right],$$

$$\mathbf{n}_{IJ}(r,s,t) = \left[n_{11IJ} \quad n_{22IJ} \quad n_{33IJ} \quad n_{12IJ} \quad n_{23IJ} \quad n_{31IJ}\right],$$

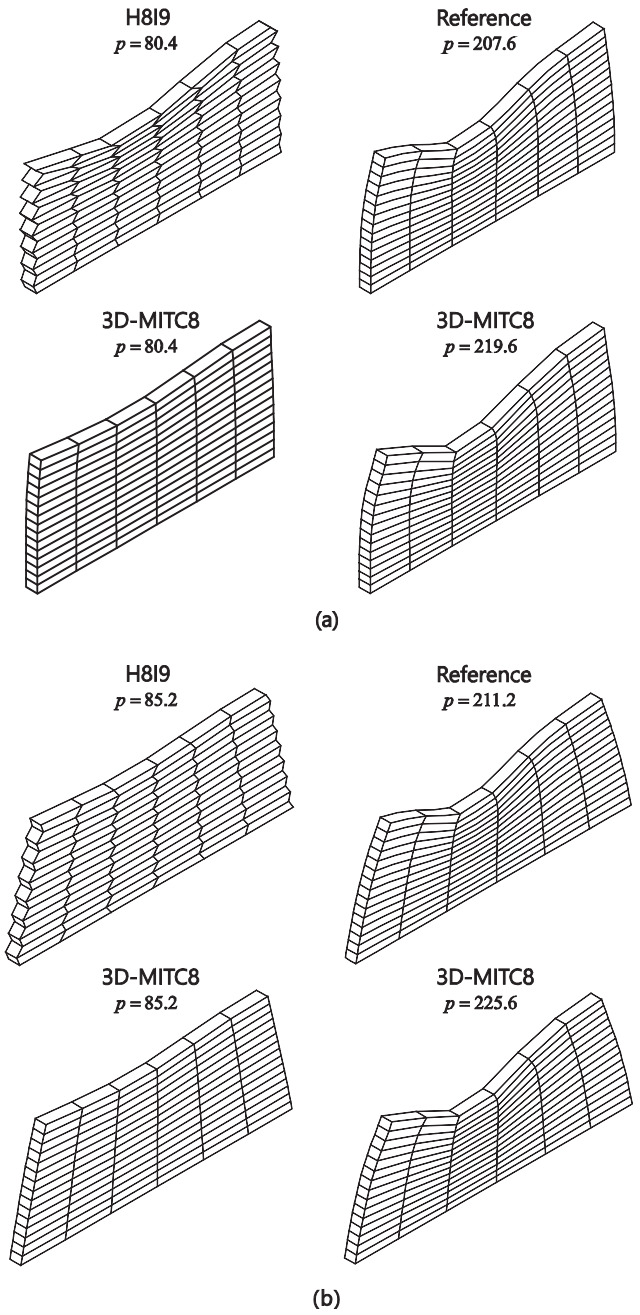

Fig. 20. Deformed shapes for the rubber blocks. (a) Rectangular block. (b) Trapezoidal block.

$$\widehat{\mathbf{G}} = \begin{pmatrix} \widehat{\mathbf{G}}_1 \\ \widehat{\mathbf{G}}_2 \\ \widehat{\mathbf{G}}_3 \\ \widehat{\mathbf{G}}_4 \\ \widehat{\mathbf{G}}_5 \\ \widehat{\mathbf{G}}_6 \end{pmatrix} = \begin{pmatrix} g_1^1 g_1^1 & g_1^2 g_1^2 & g_1^3 g_1^3 & 2g_1^1 g_1^2 & 2g_1^2 g_1^3 & 2g_1^3 g_1^1 \\ g_2^1 g_2^1 & g_2^2 g_2^2 & g_2^3 g_2^3 & 2g_2^1 g_2^2 & 2g_2^2 g_2^3 & 2g_2^3 g_2^1 \\ g_3^1 g_3^1 & g_3^2 g_3^2 & g_3^3 g_3^3 & 2g_3^1 g_3^2 & 2g_3^2 g_3^3 & 2g_3^3 g_3^1 \\ g_1^1 g_2^1 & g_1^2 g_2^2 & g_1^3 g_2^3 & g_1^1 g_2^2 + g_1^2 g_2^1 & g_1^2 g_2^3 + g_1^3 g_2^2 & g_1^3 g_2^1 + g_1^1 g_2^3 \\ g_2^1 g_3^1 & g_2^2 g_3^2 & g_2^3 g_3^3 & g_2^1 g_3^2 + g_2^2 g_3^1 & g_2^2 g_3^3 + g_2^3 g_3^2 & g_2^3 g_3^1 + g_2^1 g_3^3 \\ g_3^1 g_1^1 & g_3^2 g_1^2 & g_3^3 g_1^3 & g_3^1 g_1^2 + g_3^2 g_1^1 & g_3^2 g_1^3 + g_3^3 g_1^2 & g_3^3 g_1^1 + g_3^1 g_1^3 \end{pmatrix}, \tag{B.1}$$

$${}^0_j\widehat{\mathbf{G}} = \left(\widehat{\mathbf{C}}_1 \quad \widehat{\mathbf{C}}_2 \quad \widehat{\mathbf{C}}_3 \quad \widehat{\mathbf{C}}_4 \quad \widehat{\mathbf{C}}_5 \quad \widehat{\mathbf{C}}_6 \right).$$

We define the following representative constant vectors evaluated at the tying positions of the assumed strain components in Eq. (18)

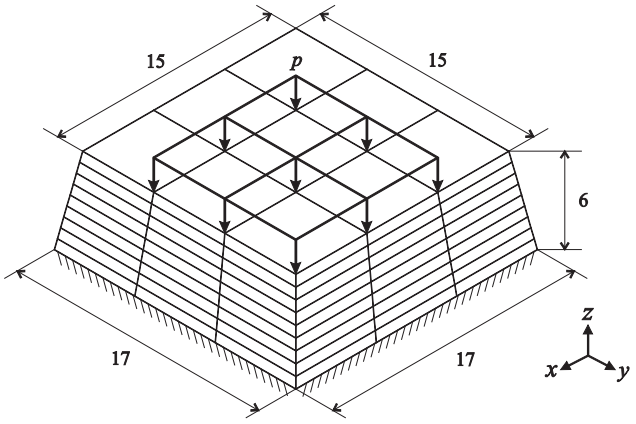

Fig. 21. A rubber panel subjected to surface loading ($3 \times 3 \times 9$ mesh, $E = 1.0 \times 10^3$ and $\nu = 0.49$).

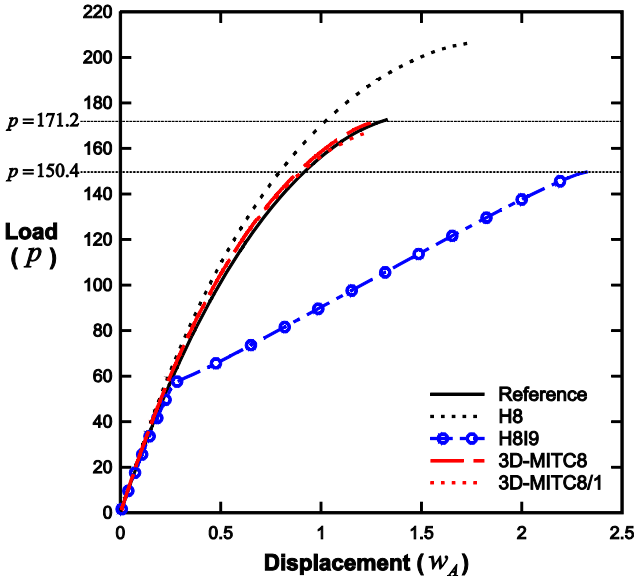

Fig. 22. Load-displacement curves for the rubber panel.

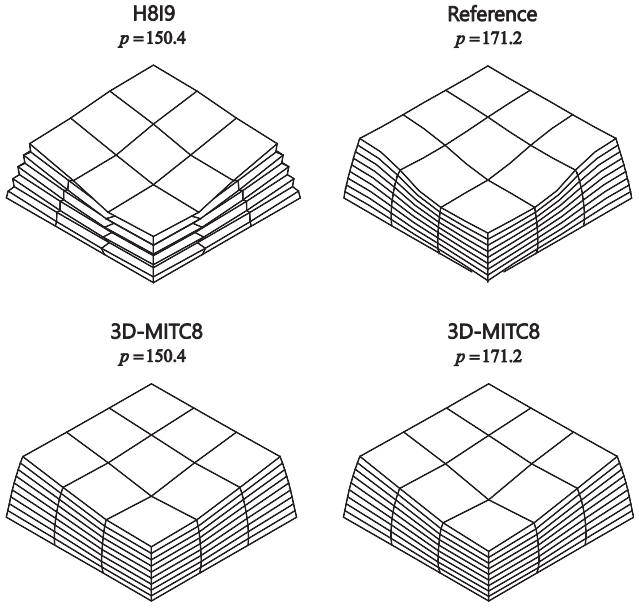

Fig. 23. Deformed shapes for the rubber panel.

$$\begin{pmatrix} \mathbf{C}_0^1 \\ \mathbf{C}_0^2 \\ \mathbf{C}_0^3 \\ \mathbf{C}_0^4 \\ \mathbf{C}_0^5 \\ \mathbf{C}_0^6 \\ \mathbf{C}_0^7 \\ \mathbf{C}_0^8 \\ \mathbf{C}_0^9 \end{pmatrix} = \frac{1}{{}^0V}\sum_{L=1}^{8} \begin{pmatrix} [1 \quad \eta_L \quad \zeta_L \quad \eta_L\zeta_L]^T \widehat{\mathbf{C}}_1^{\left(\xi_L\frac{1}{\sqrt{3}},\eta_L\frac{1}{\sqrt{3}},\zeta_L\frac{1}{\sqrt{3}}\right)} \\ [1 \quad \zeta_L \quad \xi_L \quad \zeta_L\xi_L]^T \widehat{\mathbf{C}}_2^{\left(\xi_L\frac{1}{\sqrt{3}},\eta_L\frac{1}{\sqrt{3}},\zeta_L\frac{1}{\sqrt{3}}\right)} \\ [1 \quad \xi_L \quad \eta_L \quad \xi_L\eta_L]^T \widehat{\mathbf{C}}_3^{\left(\xi_L\frac{1}{\sqrt{3}},\eta_L\frac{1}{\sqrt{3}},\zeta_L\frac{1}{\sqrt{3}}\right)} \\ [1 \quad \xi_L \quad \eta_L \quad \xi_L\eta_L]^T \widehat{\mathbf{C}}_4^{\left(\xi_L\frac{1}{\sqrt{3}},\eta_L\frac{1}{\sqrt{3}},\zeta_L\frac{1}{\sqrt{3}}\right)} \\ [1 \quad \eta_L \quad \zeta_L \quad \eta_L\zeta_L]^T \widehat{\mathbf{C}}_5^{\left(\xi_L\frac{1}{\sqrt{3}},\eta_L\frac{1}{\sqrt{3}},\zeta_L\frac{1}{\sqrt{3}}\right)} \\ [1 \quad \zeta_L \quad \xi_L \quad \zeta_L\xi_L]^T \widehat{\mathbf{C}}_6^{\left(\xi_L\frac{1}{\sqrt{3}},\eta_L\frac{1}{\sqrt{3}},\zeta_L\frac{1}{\sqrt{3}}\right)} \\ [1 \quad \xi_L \quad \eta_L \quad \xi_L\eta_L]^T \zeta_L \widehat{\mathbf{C}}_4^{\left(\xi_L\frac{1}{\sqrt{3}},\eta_L\frac{1}{\sqrt{3}},\zeta_L\frac{1}{\sqrt{3}}\right)} \\ [1 \quad \eta_L \quad \zeta_L \quad \eta_L\zeta_L]^T \xi_L \widehat{\mathbf{C}}_5^{\left(\xi_L\frac{1}{\sqrt{3}},\eta_L\frac{1}{\sqrt{3}},\zeta_L\frac{1}{\sqrt{3}}\right)} \\ [1 \quad \zeta_L \quad \xi_L \quad \zeta_L\xi_L]^T \eta_L \widehat{\mathbf{C}}_6^{\left(\xi_L\frac{1}{\sqrt{3}},\eta_L\frac{1}{\sqrt{3}},\zeta_L\frac{1}{\sqrt{3}}\right)} \end{pmatrix},$$

$${}^0V = \sum_{L=1}^{8} {}^0j\left(\xi_L\tfrac{1}{\sqrt{3}},\eta_L\tfrac{1}{\sqrt{3}},\zeta_L\tfrac{1}{\sqrt{3}}\right),$$

$$\begin{pmatrix} \mathbf{G}_1^1 & \mathbf{G}_2^1 & \mathbf{G}_3^1 \\ \mathbf{G}_1^2 & \mathbf{G}_2^2 & \mathbf{G}_3^2 \\ \mathbf{G}_1^3 & \mathbf{G}_2^3 & \mathbf{G}_3^3 \\ \mathbf{G}_1^4 & \mathbf{G}_2^4 & \mathbf{G}_3^4 \end{pmatrix} = \sum_{L=1}^{4} \begin{pmatrix} 1 \\ \hat{\xi}_L \\ \hat{\eta}_L \\ \hat{\xi}_L\hat{\eta}_L \end{pmatrix} \begin{pmatrix} \widehat{\mathbf{G}}_1^{\left(0,\hat{\xi}_L\frac{1}{\sqrt{3}},\hat{\eta}_L\frac{1}{\sqrt{3}}\right)} & \widehat{\mathbf{G}}_2^{\left(\hat{\eta}_L\frac{1}{\sqrt{3}}0,\hat{\xi}_L\frac{1}{\sqrt{3}}\right)} & \widehat{\mathbf{G}}_3^{\left(\hat{\xi}_L\frac{1}{\sqrt{3}},\hat{\eta}_L\frac{1}{\sqrt{3}}0\right)} \end{pmatrix},$$

$$\begin{pmatrix} \mathbf{G}_4^1 & \mathbf{G}_5^1 & \mathbf{G}_6^1 \\ \mathbf{G}_4^2 & \mathbf{G}_5^2 & \mathbf{G}_6^2 \end{pmatrix} = \sum_{L=1}^{2} \begin{pmatrix} 1 \\ \hat{\zeta}_L \end{pmatrix} \begin{pmatrix} \widehat{\mathbf{G}}_4^{(0,0,\hat{\zeta}_L)} & \widehat{\mathbf{G}}_5^{(\hat{\zeta}_L,0,0)} & \widehat{\mathbf{G}}_6^{(0,\hat{\zeta}_L,0)} \end{pmatrix},$$

$$\begin{pmatrix} \mathbf{H}_4^1 & \mathbf{H}_5^1 & \mathbf{H}_6^1 \\ \mathbf{H}_4^2 & \mathbf{H}_5^2 & \mathbf{H}_6^2 \\ \mathbf{H}_4^3 & \mathbf{H}_5^3 & \mathbf{H}_6^3 \\ \mathbf{H}_4^4 & \mathbf{H}_5^4 & \mathbf{H}_6^4 \\ \mathbf{H}_4^5 & \mathbf{H}_5^5 & \mathbf{H}_6^5 \\ \mathbf{H}_4^6 & \mathbf{H}_5^6 & \mathbf{H}_6^6 \\ \mathbf{H}_4^7 & \mathbf{H}_5^7 & \mathbf{H}_6^7 \\ \mathbf{H}_4^8 & \mathbf{H}_5^8 & \mathbf{H}_6^8 \end{pmatrix} = \sum_{L=1}^{4}\sum_{M=1}^{2} \begin{pmatrix} 1 \\ \hat{\xi}_L \\ \hat{\eta}_L \\ \hat{\xi}_L\hat{\eta}_L \\ \hat{\zeta}_M \\ \hat{\xi}_L\hat{\zeta}_M \\ \hat{\eta}_L\hat{\zeta}_M \\ \hat{\xi}_L\hat{\eta}_L\hat{\zeta}_M \end{pmatrix} \begin{pmatrix} \widehat{\mathbf{G}}_4^{\left(\hat{\xi}_L\frac{1}{\sqrt{3}},\hat{\eta}_L\frac{1}{\sqrt{3}},\hat{\zeta}_M\right)} & \widehat{\mathbf{G}}_5^{\left(\hat{\zeta}_M,\hat{\xi}_L\frac{1}{\sqrt{3}},\hat{\eta}_L\frac{1}{\sqrt{3}}\right)} & \widehat{\mathbf{G}}_6^{\left(\hat{\eta}_L\frac{1}{\sqrt{3}},\hat{\zeta}_M,\hat{\xi}_L\frac{1}{\sqrt{3}}\right)} \end{pmatrix}, \tag{B.2}$$

in which the signs are $[\hat{\zeta}_1 \quad \hat{\zeta}_2] = [1 \quad -1]$, $[\hat{\xi}_1 \quad \hat{\xi}_2 \quad \hat{\xi}_3 \quad \hat{\xi}_4] = [-1 \quad 1 \quad 1 \quad -1]$ and $[\hat{\eta}_1 \quad \hat{\eta}_2 \quad \hat{\eta}_3 \quad \hat{\eta}_4] = [-1 \quad -1 \quad 1 \quad 1]$. We note that the constants in Eq. (B.2) are calculated only once for each element.

We define the following representative nodal constants

$$\mathbf{n}_0^0|_{IJ} = \begin{bmatrix} n_{IJ}^{[1|1]} & n_{IJ}^{[2|2]} & n_{IJ}^{[3|3]} & n_{IJ}^{[1|2]} & n_{IJ}^{[2|3]} & n_{IJ}^{[1|3]} \end{bmatrix},$$

$$\begin{pmatrix} \mathbf{n}_0^1|_{IJ}^T \\ \mathbf{n}_0^2|_{IJ}^T \\ \mathbf{n}_0^3|_{IJ}^T \end{pmatrix} = \frac{1}{8}\sum_{L=1}^{8} \begin{pmatrix} [1 \quad \xi_L \quad \eta_L \quad \xi_L\eta_L]\tilde{n}_{rrIJ}^{\left(0,\xi_L\frac{1}{\sqrt{3}},\eta_L\frac{1}{\sqrt{3}}\right)} \\ [1 \quad \xi_L \quad \eta_L \quad \xi_L\eta_L]\tilde{n}_{ssIJ}^{\left(\eta_L\frac{1}{\sqrt{3}}0,\xi_L\frac{1}{\sqrt{3}}\right)} \\ [1 \quad \xi_L \quad \eta_L \quad \xi_L\eta_L]\tilde{n}_{ttIJ}^{\left(\xi_L\frac{1}{\sqrt{3}},\eta_L\frac{1}{\sqrt{3}}0\right)} \end{pmatrix}$$

$$= \begin{pmatrix} n_{IJ}^{[1|1]} + \frac{1}{3}n_{IJ}^{[4|4]} + \frac{1}{3}n_{IJ}^{[6|6]} + \frac{1}{9}\tilde{n}_{IJ}^{[7|7]} & \frac{2}{\sqrt{3}}\left(n_{IJ}^{[1|4]} + \frac{1}{3}\tilde{n}_{IJ}^{[6|7]}\right) & \frac{2}{\sqrt{3}}\left(n_{IJ}^{[1|6]} + \frac{1}{3}\tilde{n}_{IJ}^{[4|7]}\right) & \frac{2}{3}\left(\tilde{n}_{IJ}^{[1|7]} + n_{IJ}^{[4|6]}\right) \\ n_{IJ}^{[2|2]} + \frac{1}{3}n_{IJ}^{[5|5]} + \frac{1}{3}n_{IJ}^{[4|4]} + \frac{1}{9}\tilde{n}_{IJ}^{[7|7]} & \frac{2}{\sqrt{3}}\left(n_{IJ}^{[2|5]} + \frac{1}{3}\tilde{n}_{IJ}^{[4|7]}\right) & \frac{2}{\sqrt{3}}\left(n_{IJ}^{[2|4]} + \frac{1}{3}\tilde{n}_{IJ}^{[5|7]}\right) & \frac{2}{3}\left(\tilde{n}_{IJ}^{[2|7]} + n_{IJ}^{[4|5]}\right) \\ n_{IJ}^{[3|3]} + \frac{1}{3}n_{IJ}^{[6|6]} + \frac{1}{3}n_{IJ}^{[5|5]} + \frac{1}{9}\tilde{n}_{IJ}^{[7|7]} & \frac{2}{\sqrt{3}}\left(n_{IJ}^{[3|6]} + \frac{1}{3}\tilde{n}_{IJ}^{[5|7]}\right) & \frac{2}{\sqrt{3}}\left(n_{IJ}^{[3|5]} + \frac{1}{3}\tilde{n}_{IJ}^{[6|7]}\right) & \frac{2}{3}\left(\tilde{n}_{IJ}^{[3|7]} + n_{IJ}^{[5|6]}\right) \end{pmatrix},$$

$$\begin{pmatrix} \mathbf{n}_0^4|_{IJ}^T \\ \mathbf{n}_0^5|_{IJ}^T \\ \mathbf{n}_0^6|_{IJ}^T \end{pmatrix} = \frac{1}{8}\sum_{L=1}^{8} \begin{pmatrix} [1 \quad \xi_L \quad \eta_L \quad \xi_L\eta_L]\tilde{n}_{rsIJ}^{\left(\xi_L\frac{1}{\sqrt{3}},\eta_L\frac{1}{\sqrt{3}},\zeta_L\frac{1}{\sqrt{3}}\right)} \\ [1 \quad \eta_L \quad \zeta_L \quad \eta_L\zeta_L]\tilde{n}_{stIJ}^{\left(\xi_L\frac{1}{\sqrt{3}},\eta_L\frac{1}{\sqrt{3}},\zeta_L\frac{1}{\sqrt{3}}\right)} \\ [1 \quad \zeta_L \quad \xi_L \quad \zeta_L\xi_L]\tilde{n}_{trIJ}^{\left(\xi_L\frac{1}{\sqrt{3}},\eta_L\frac{1}{\sqrt{3}},\zeta_L\frac{1}{\sqrt{3}}\right)} \end{pmatrix}$$

$$= \begin{pmatrix} n_{IJ}^{[1|2]} + \frac{1}{3}n_{IJ}^{[5|6]} & \frac{1}{\sqrt{3}}\left(n_{IJ}^{[1|4]} + \frac{1}{3}\tilde{n}_{IJ}^{[6|7]}\right) & \frac{1}{\sqrt{3}}\left(n_{IJ}^{[2|4]} + \frac{1}{3}\tilde{n}_{IJ}^{[5|7]}\right) & \frac{1}{3}\left(n_{IJ}^{[4|4]} + \frac{1}{3}\tilde{n}_{IJ}^{[7|7]}\right) \\ n_{IJ}^{[2|3]} + \frac{1}{3}n_{IJ}^{[4|6]} & \frac{1}{\sqrt{3}}\left(n_{IJ}^{[2|5]} + \frac{1}{3}\tilde{n}_{IJ}^{[4|7]}\right) & \frac{1}{\sqrt{3}}\left(n_{IJ}^{[3|5]} + \frac{1}{3}\tilde{n}_{IJ}^{[6|7]}\right) & \frac{1}{3}\left(n_{IJ}^{[5|5]} + \frac{1}{3}\tilde{n}_{IJ}^{[7|7]}\right) \\ n_{IJ}^{[1|3]} + \frac{1}{3}n_{IJ}^{[4|5]} & \frac{1}{\sqrt{3}}\left(n_{IJ}^{[3|6]} + \frac{1}{3}\tilde{n}_{IJ}^{[5|7]}\right) & \frac{1}{\sqrt{3}}\left(n_{IJ}^{[1|6]} + \frac{1}{3}\tilde{n}_{IJ}^{[4|7]}\right) & \frac{1}{3}\left(n_{IJ}^{[6|6]} + \frac{1}{3}\tilde{n}_{IJ}^{[7|7]}\right) \end{pmatrix},$$

$$\begin{pmatrix} \mathbf{n}_0^7|_{IJ}^T \\ \mathbf{n}_0^8|_{IJ}^T \\ \mathbf{n}_0^9|_{IJ}^T \end{pmatrix} = \frac{1}{8}\sum_{L=1}^{8} \begin{pmatrix} [1 \quad \xi_L \quad \eta_L \quad \xi_L\eta_L]\zeta_L \tilde{n}_{rsIJ}^{\left(\xi_L\frac{1}{\sqrt{3}},\eta_L\frac{1}{\sqrt{3}},\zeta_L\frac{1}{\sqrt{3}}\right)} \\ [1 \quad \eta_L \quad \zeta_L \quad \eta_L\zeta_L]\xi_L \tilde{n}_{stIJ}^{\left(\xi_L\frac{1}{\sqrt{3}},\eta_L\frac{1}{\sqrt{3}},\zeta_L\frac{1}{\sqrt{3}}\right)} \\ [1 \quad \zeta_L \quad \xi_L \quad \zeta_L\xi_L]\eta_L \tilde{n}_{trIJ}^{\left(\xi_L\frac{1}{\sqrt{3}},\eta_L\frac{1}{\sqrt{3}},\zeta_L\frac{1}{\sqrt{3}}\right)} \end{pmatrix}$$

$$= \begin{pmatrix} \frac{1}{\sqrt{3}}\left(n_{IJ}^{[1|5]} + n_{IJ}^{[2|6]}\right) & \frac{1}{3}\left(n_{IJ}^{[4|6]} + \tilde{n}_{IJ}^{[1|7]}\right) & \frac{1}{3}\left(n_{IJ}^{[4|5]} + \tilde{n}_{IJ}^{[2|7]}\right) & \frac{2}{3\sqrt{3}}\tilde{n}_{IJ}^{[4|7]} \\ \frac{1}{\sqrt{3}}\left(n_{IJ}^{[2|6]} + n_{IJ}^{[3|4]}\right) & \frac{1}{3}\left(n_{IJ}^{[4|5]} + \tilde{n}_{IJ}^{[2|7]}\right) & \frac{1}{3}\left(n_{IJ}^{[5|6]} + \tilde{n}_{IJ}^{[3|7]}\right) & \frac{2}{3\sqrt{3}}\tilde{n}_{IJ}^{[5|7]} \\ \frac{1}{\sqrt{3}}\left(n_{IJ}^{[3|4]} + n_{IJ}^{[1|5]}\right) & \frac{1}{3}\left(n_{IJ}^{[5|6]} + \tilde{n}_{IJ}^{[3|7]}\right) & \frac{1}{3}\left(n_{IJ}^{[4|6]} + \tilde{n}_{IJ}^{[1|7]}\right) & \frac{2}{3\sqrt{3}}\tilde{n}_{IJ}^{[6|7]} \end{pmatrix},$$

$$\left(\mathbf{E}_1|_{IJ} \quad \mathbf{E}_2|_{IJ} \quad \mathbf{E}_3|_{IJ}\right) = \frac{1}{4}\sum_{L=1}^{4} \begin{pmatrix} 1 \\ \hat{\xi}_L \\ \hat{\eta}_L \\ \hat{\xi}_L\hat{\eta}_L \end{pmatrix} \left(\mathbf{n}_{IJ}^{\left(0,\hat{\xi}_L\frac{1}{\sqrt{3}},\hat{\eta}_L\frac{1}{\sqrt{3}}\right)^T} \quad \mathbf{n}_{IJ}^{\left(\hat{\eta}_L\frac{1}{\sqrt{3}},0,\hat{\xi}_L\frac{1}{\sqrt{3}}\right)^T} \quad \mathbf{n}_{IJ}^{\left(\hat{\xi}_L\frac{1}{\sqrt{3}},\hat{\eta}_L\frac{1}{\sqrt{3}},0\right)^T} \right),$$

$$\mathbf{E}_1|_{IJ} = \begin{pmatrix} \mathbf{n}_0^0|_{IJ}^T + \frac{1}{3}\left[n_{IJ}^{[4|4]} + n_{IJ}^{[6|6]} + \frac{1}{3}n_{IJ}^{[7|7]} \quad n_{IJ}^{[5|5]} \quad n_{IJ}^{[5|5]} \quad n_{IJ}^{[5|6]} \quad 0 \quad n_{IJ}^{[4|5]} \right]^T \\ \frac{1}{\sqrt{3}}\left[2n_{IJ}^{[1|4]} + \frac{2}{3}n_{IJ}^{[6|7]} \quad 0 \quad 2n_{IJ}^{[3|5]} \quad n_{IJ}^{[2|4]} + \frac{1}{3}n_{IJ}^{[5|7]} \quad n_{IJ}^{[2|5]} \quad n_{IJ}^{[3|4]} + n_{IJ}^{[1|5]} \right]^T \\ \frac{1}{\sqrt{3}}\left[2n_{IJ}^{[1|6]} + \frac{2}{3}n_{IJ}^{[4|7]} \quad 2n_{IJ}^{[2|5]} \quad 0 \quad n_{IJ}^{[1|5]} + n_{IJ}^{[2|6]} \quad n_{IJ}^{[3|5]} \quad n_{IJ}^{[3|6]} + \frac{1}{3}n_{IJ}^{[5|7]} \right]^T \\ \frac{1}{3}\left[2n_{IJ}^{[1|7]} + 2n_{IJ}^{[4|6]} \quad 0 \quad 0 \quad n_{IJ}^{[4|5]} + n_{IJ}^{[2|7]} \quad n_{IJ}^{[5|5]} \quad n_{IJ}^{[5|6]} + n_{IJ}^{[3|7]} \right]^T \end{pmatrix},$$

$$\mathbf{E}_2|_{IJ} = \begin{pmatrix} \mathbf{n}_0^0|_{IJ}^T + \frac{1}{3}\left[n_{IJ}^{[6|6]} \quad n_{IJ}^{[5|5]} + n_{IJ}^{[4|4]} + \frac{1}{3}n_{IJ}^{[7|7]} \quad n_{IJ}^{[6|6]} \quad n_{IJ}^{[5|6]} \quad n_{IJ}^{[4|6]} \quad 0 \right]^T \\ \frac{1}{\sqrt{3}}\left[2n_{IJ}^{[1|6]} \quad 2n_{IJ}^{[2|5]} + \frac{2}{3}n_{IJ}^{[4|7]} \quad 0 \quad n_{IJ}^{[1|5]} + n_{IJ}^{[2|6]} \quad n_{IJ}^{[3|5]} + \frac{1}{3}n_{IJ}^{[6|7]} \quad n_{IJ}^{[3|6]} \right]^T \\ \frac{1}{\sqrt{3}}\left[0 \quad 2n_{IJ}^{[2|4]} + \frac{2}{3}n_{IJ}^{[5|7]} \quad 2n_{IJ}^{[3|6]} \quad n_{IJ}^{[1|4]} + \frac{1}{3}n_{IJ}^{[6|7]} \quad n_{IJ}^{[2|6]} + n_{IJ}^{[3|4]} \quad n_{IJ}^{[1|6]} \right]^T \\ \frac{1}{3}\left[0 \quad 2n_{IJ}^{[2|7]} + 2n_{IJ}^{[4|5]} \quad 0 \quad n_{IJ}^{[4|6]} + n_{IJ}^{[1|7]} \quad n_{IJ}^{[5|6]} + n_{IJ}^{[3|7]} \quad n_{IJ}^{[6|6]} \right]^T \end{pmatrix},$$

$$\mathbf{E}_3|_{IJ} = \begin{pmatrix} \mathbf{n}_0^0|_{IJ}^T + \frac{1}{3}\left[n_{IJ}^{[4|4]} \quad n_{IJ}^{[4|4]} \quad n_{IJ}^{[6|6]} + n_{IJ}^{[5|5]} + \frac{1}{3}n_{IJ}^{[7|7]} \quad 0 \quad n_{IJ}^{[4|6]} \quad n_{IJ}^{[4|5]} \right]^T \\ \frac{1}{\sqrt{3}}\left[0 \quad 2n_{IJ}^{[2|4]} \quad 2n_{IJ}^{[3|6]} + \frac{2}{3}n_{IJ}^{[5|7]} \quad n_{IJ}^{[1|4]} \quad n_{IJ}^{[2|6]} + n_{IJ}^{[3|4]} \quad n_{IJ}^{[1|6]} + \frac{1}{3}n_{IJ}^{[4|7]} \right]^T \\ \frac{1}{\sqrt{3}}\left[2n_{IJ}^{[1|4]} \quad 0 \quad 2n_{IJ}^{[3|5]} + \frac{2}{3}n_{IJ}^{[6|7]} \quad n_{IJ}^{[2|4]} \quad n_{IJ}^{[2|5]} + \frac{1}{3}n_{IJ}^{[4|7]} \quad n_{IJ}^{[3|4]} + n_{IJ}^{[1|5]} \right]^T \\ \frac{1}{3}\left[0 \quad 0 \quad 2n_{IJ}^{[3|7]} + 2n_{IJ}^{[5|6]} \quad n_{IJ}^{[4|4]} \quad n_{IJ}^{[4|5]} + n_{IJ}^{[2|7]} \quad n_{IJ}^{[4|6]} + n_{IJ}^{[1|7]} \right]^T \end{pmatrix},$$

$$\begin{pmatrix} \mathbf{n}_4^1|_{IJ} \\ \mathbf{n}_4^2|_{IJ} \end{pmatrix} = \frac{1}{2}\sum_{L=1}^{2} \begin{pmatrix} 1 \\ \hat{\zeta}_L \end{pmatrix} \mathbf{n}_{IJ}^{(0,0,\hat{\zeta}_L)^T} = \begin{pmatrix} \mathbf{n}_0^0|_{IJ}^T + \left[n_{IJ}^{[6|6]} \quad n_{IJ}^{[5|5]} \quad 0 \quad n_{IJ}^{[5|6]} \quad 0 \quad 0 \right]^T \\ \left[2n_{IJ}^{[1|6]} \quad 2n_{IJ}^{[2|5]} \quad 0 \quad n_{IJ}^{[1|5]} + n_{IJ}^{[2|6]} \quad n_{IJ}^{[3|5]} \quad n_{IJ}^{[3|6]} \right]^T \end{pmatrix},$$

$$\begin{pmatrix} \mathbf{n}_5^1|_{IJ} \\ \mathbf{n}_5^2|_{IJ} \end{pmatrix} = \frac{1}{2}\sum_{L=1}^{2} \begin{pmatrix} 1 \\ \hat{\zeta}_L \end{pmatrix} \mathbf{n}_{IJ}^{(\hat{\zeta}_L,0,0)^T} = \begin{pmatrix} \mathbf{n}_0^0|_{IJ}^T + \left[0 \quad n_{IJ}^{[4|4]} \quad n_{IJ}^{[6|6]} \quad 0 \quad n_{IJ}^{[4|6]} \quad 0 \right]^T \\ \left[0 \quad 2n_{IJ}^{[2|4]} \quad 2n_{IJ}^{[3|6]} \quad n_{IJ}^{[1|4]} \quad n_{IJ}^{[2|6]} + n_{IJ}^{[3|4]} \quad n_{IJ}^{[1|6]} \right]^T \end{pmatrix},$$

$$\begin{pmatrix} \mathbf{n}_6^1|_{IJ} \\ \mathbf{n}_6^2|_{IJ} \end{pmatrix} = \frac{1}{2}\sum_{L=1}^{2} \begin{pmatrix} 1 \\ \hat{\zeta}_L \end{pmatrix} \mathbf{n}_{IJ}^{(0,\hat{\zeta}_L,0)^T} = \begin{pmatrix} \mathbf{n}_0^0|_{IJ}^T + \left[n_{IJ}^{[4|4]} \quad 0 \quad n_{IJ}^{[5|5]} \quad 0 \quad 0 \quad n_{IJ}^{[4|5]} \right]^T \\ \left[2n_{IJ}^{[1|4]} \quad 0 \quad 2n_{IJ}^{[3|5]} \quad n_{IJ}^{[2|4]} \quad n_{IJ}^{[2|5]} \quad n_{IJ}^{[3|4]} + n_{IJ}^{[1|5]} \right]^T \end{pmatrix},$$

$$\mathbf{s}_0^0|_{IJ} = \mathbf{n}_0^0|_{IJ} + \frac{1}{3}\left[n_{IJ}^{[4|4]} + n_{IJ}^{[6|6]} \quad n_{IJ}^{[5|5]} + n_{IJ}^{[4|4]} \quad n_{IJ}^{[6|6]} + n_{IJ}^{[5|5]} \quad n_{IJ}^{[5|6]} \quad n_{IJ}^{[4|6]} \quad n_{IJ}^{[4|5]} \right],$$

$$\left(\mathbf{S}_4|_{IJ} \quad \mathbf{S}_5|_{IJ} \quad \mathbf{S}_6|_{IJ}\right) = \frac{1}{8}\sum_{L=1}^{4}\sum_{M=1}^{2}\begin{pmatrix} 1 \\ \hat{\xi}_L \\ \hat{\eta}_L \\ \hat{\xi}_L\hat{\eta}_L \\ \hat{\zeta}_M \\ \hat{\xi}_L\hat{\zeta}_M \\ \hat{\eta}_L\hat{\zeta}_M \\ \hat{\xi}_L\hat{\eta}_L\hat{\zeta}_M \end{pmatrix}\left(\mathbf{n}_{IJ}^{\left(\hat{\xi}_L\frac{1}{\sqrt{3}},\hat{\eta}_L\frac{1}{\sqrt{3}},\hat{\zeta}_M\right)^T} \quad \mathbf{n}_{IJ}^{\left(\hat{\zeta}_M,\hat{\xi}_L\frac{1}{\sqrt{3}},\hat{\eta}_L\frac{1}{\sqrt{3}}\right)^T} \quad \mathbf{n}_{IJ}^{\left(\hat{\eta}_L\frac{1}{\sqrt{3}},\hat{\zeta}_M,\hat{\xi}_L\frac{1}{\sqrt{3}}\right)^T}\right),$$

$$\mathbf{S}_4|_{IJ} = \begin{pmatrix} \mathbf{s}_0^0|_{IJ}^T + \frac{1}{3}\left[2n_{IJ}^{[6|6]} + n_{IJ}^{[7|7]} \quad 2n_{IJ}^{[5|5]} + n_{IJ}^{[7|7]} \quad \frac{1}{3}n_{IJ}^{[7|7]} \quad 2n_{IJ}^{[5|6]} \quad 0 \quad 0\right]^T \\ \frac{1}{\sqrt{3}}\left[0 \quad 2\left(n_{IJ}^{[2|4]} + n_{IJ}^{[5|7]}\right) \quad 2\left(n_{IJ}^{[3|6]} + \frac{1}{3}n_{IJ}^{[5|7]}\right) \quad n_{IJ}^{[1|4]} + n_{IJ}^{[6|7]} \quad n_{IJ}^{[2|6]} + n_{IJ}^{[3|4]} \quad n_{IJ}^{[1|6]} + \frac{1}{3}n_{IJ}^{[4|7]}\right]^T \\ \frac{1}{\sqrt{3}}\left[2\left(n_{IJ}^{[1|4]} + n_{IJ}^{[6|7]}\right) \quad 0 \quad 2\left(n_{IJ}^{[3|5]} + \frac{1}{3}n_{IJ}^{[6|7]}\right) \quad n_{IJ}^{[2|4]} + n_{IJ}^{[5|7]} \quad n_{IJ}^{[2|5]} + \frac{1}{3}n_{IJ}^{[4|7]} \quad n_{IJ}^{[3|4]} + n_{IJ}^{[1|5]}\right]^T \\ \frac{1}{3}\left[0 \quad 0 \quad 2\left(n_{IJ}^{[3|7]} + \frac{1}{3}n_{IJ}^{[5|6]}\right) \quad n_{IJ}^{[4|4]} + n_{IJ}^{[7|7]} \quad n_{IJ}^{[4|5]} + n_{IJ}^{[2|7]} \quad n_{IJ}^{[4|6]} + n_{IJ}^{[1|7]}\right]^T \\ \left[2\left(n_{IJ}^{[1|6]} + \frac{1}{3}n_{IJ}^{[4|7]}\right) \quad 2\left(n_{IJ}^{[2|5]} + \frac{1}{3}n_{IJ}^{[4|7]}\right) \quad 0 \quad n_{IJ}^{[1|5]} + n_{IJ}^{[2|6]} \quad n_{IJ}^{[3|5]} + \frac{1}{3}n_{IJ}^{[6|7]} \quad n_{IJ}^{[3|6]} + \frac{1}{3}n_{IJ}^{[5|7]}\right]^T \\ \frac{1}{\sqrt{3}}\left[0 \quad 2\left(n_{IJ}^{[2|7]} + n_{IJ}^{[4|5]}\right) \quad 0 \quad n_{IJ}^{[4|6]} + n_{IJ}^{[1|7]} \quad n_{IJ}^{[5|6]} + n_{IJ}^{[3|7]} \quad n_{IJ}^{[6|6]} + \frac{1}{3}n_{IJ}^{[7|7]}\right]^T \\ \frac{1}{\sqrt{3}}\left[2\left(n_{IJ}^{[1|7]} + n_{IJ}^{[4|6]}\right) \quad 0 \quad 0 \quad n_{IJ}^{[4|5]} + n_{IJ}^{[2|7]} \quad n_{IJ}^{[5|5]} + \frac{1}{3}n_{IJ}^{[7|7]} \quad n_{IJ}^{[5|6]} + n_{IJ}^{[3|7]}\right]^T \\ \frac{2}{3}\left[0 \quad 0 \quad 0 \quad n_{IJ}^{[4|7]} \quad n_{IJ}^{[5|7]} \quad n_{IJ}^{[6|7]}\right]^T \end{pmatrix},$$

$$\mathbf{S}_5|_{IJ} = \begin{pmatrix} \mathbf{s}_0^0|_{IJ}^T + \frac{1}{3}\left[\frac{1}{3}n_{IJ}^{[7|7]} \quad 2n_{IJ}^{[4|4]} + n_{IJ}^{[7|7]} \quad 2n_{IJ}^{[6|6]} + n_{IJ}^{[7|7]} \quad 0 \quad 2n_{IJ}^{[4|6]} \quad 0\right]^T \\ \frac{1}{\sqrt{3}}\left[2\left(n_{IJ}^{[1|4]} + \frac{1}{3}n_{IJ}^{[6|7]}\right) \quad 0 \quad 2\left(n_{IJ}^{[3|5]} + n_{IJ}^{[6|7]}\right) \quad n_{IJ}^{[2|4]} + \frac{1}{3}n_{IJ}^{[5|7]} \quad n_{IJ}^{[2|5]} + n_{IJ}^{[4|7]} \quad n_{IJ}^{[3|4]} + n_{IJ}^{[1|5]}\right]^T \\ \frac{1}{\sqrt{3}}\left[2\left(n_{IJ}^{[1|6]} + \frac{1}{3}n_{IJ}^{[4|7]}\right) \quad 2\left(n_{IJ}^{[2|5]} + n_{IJ}^{[4|7]}\right) \quad 0 \quad n_{IJ}^{[1|5]} + n_{IJ}^{[2|6]} \quad n_{IJ}^{[3|5]} + n_{IJ}^{[6|7]} \quad n_{IJ}^{[3|6]} + \frac{1}{3}n_{IJ}^{[5|7]}\right]^T \\ \frac{1}{3}\left[2\left(n_{IJ}^{[1|7]} + n_{IJ}^{[4|6]}\right) \quad 0 \quad 0 \quad n_{IJ}^{[4|5]} + n_{IJ}^{[2|7]} \quad n_{IJ}^{[5|5]} + n_{IJ}^{[7|7]} \quad n_{IJ}^{[5|6]} + n_{IJ}^{[3|7]}\right]^T \\ \left[0 \quad 2\left(n_{IJ}^{[2|4]} + \frac{1}{3}n_{IJ}^{[5|7]}\right) \quad 2\left(n_{IJ}^{[3|6]} + \frac{1}{3}n_{IJ}^{[5|7]}\right) \quad n_{IJ}^{[1|4]} + \frac{1}{3}n_{IJ}^{[6|7]} \quad n_{IJ}^{[2|6]} + n_{IJ}^{[3|4]} \quad n_{IJ}^{[1|6]} + \frac{1}{3}n_{IJ}^{[4|7]}\right]^T \\ \frac{1}{\sqrt{3}}\left[0 \quad 0 \quad 2\left(n_{IJ}^{[3|7]} + n_{IJ}^{[5|6]}\right) \quad n_{IJ}^{[4|4]} + \frac{1}{3}n_{IJ}^{[7|7]} \quad n_{IJ}^{[4|5]} + n_{IJ}^{[2|7]} \quad n_{IJ}^{[4|6]} + n_{IJ}^{[1|7]}\right]^T \\ \frac{1}{\sqrt{3}}\left[0 \quad 2\left(n_{IJ}^{[2|7]} + n_{IJ}^{[4|5]}\right) \quad 0 \quad n_{IJ}^{[4|6]} + n_{IJ}^{[1|7]} \quad n_{IJ}^{[5|6]} + n_{IJ}^{[3|7]} \quad n_{IJ}^{[6|6]} + \frac{1}{3}n_{IJ}^{[7|7]}\right]^T \\ \frac{2}{3}\left[0 \quad 0 \quad 0 \quad n_{IJ}^{[4|7]} \quad n_{IJ}^{[5|7]} \quad n_{IJ}^{[6|7]}\right]^T \end{pmatrix},$$

$$\mathbf{S}_6|_{IJ} = \begin{pmatrix} \mathbf{s}_0^0|_{IJ}^T + \frac{1}{3}\left[2n_{IJ}^{[4|4]} + n_{IJ}^{[7|7]} \quad \frac{1}{3}n_{IJ}^{[7|7]} \quad 2n_{IJ}^{[5|5]} + n_{IJ}^{[7|7]} \quad 0 \quad 0 \quad 2n_{IJ}^{[4|5]}\right]^T \\ \frac{1}{\sqrt{3}}\left[2\left(n_{IJ}^{[1|6]} + n_{IJ}^{[4|7]}\right) \quad 2\left(n_{IJ}^{[2|5]} + \frac{1}{3}n_{IJ}^{[4|7]}\right) \quad 0 \quad n_{IJ}^{[1|5]} + n_{IJ}^{[2|6]} \quad n_{IJ}^{[3|5]} + \frac{1}{3}n_{IJ}^{[6|7]} \quad n_{IJ}^{[3|6]} + n_{IJ}^{[5|7]}\right]^T \\ \frac{1}{\sqrt{3}}\left[0 \quad 2\left(n_{IJ}^{[2|4]} + \frac{1}{3}n_{IJ}^{[5|7]}\right) \quad 2\left(n_{IJ}^{[3|6]} + n_{IJ}^{[5|7]}\right) \quad n_{IJ}^{[1|4]} + \frac{1}{3}n_{IJ}^{[6|7]} \quad n_{IJ}^{[2|6]} + n_{IJ}^{[3|4]} \quad n_{IJ}^{[1|6]} + n_{IJ}^{[4|7]}\right]^T \\ \frac{1}{3}\left[0 \quad 2\left(n_{IJ}^{[2|7]} + n_{IJ}^{[4|5]}\right) \quad 0 \quad n_{IJ}^{[4|6]} + n_{IJ}^{[1|7]} \quad n_{IJ}^{[5|6]} + n_{IJ}^{[3|7]} \quad n_{IJ}^{[6|6]} + n_{IJ}^{[7|7]}\right]^T \\ \left[2\left(n_{IJ}^{[1|4]} + \frac{1}{3}n_{IJ}^{[6|7]}\right) \quad 0 \quad 2\left(n_{IJ}^{[3|5]} + \frac{1}{3}n_{IJ}^{[6|7]}\right) \quad n_{IJ}^{[2|4]} + \frac{1}{3}n_{IJ}^{[5|7]} \quad n_{IJ}^{[2|5]} + \frac{1}{3}n_{IJ}^{[4|7]} \quad n_{IJ}^{[3|4]} + n_{IJ}^{[1|5]}\right]^T \\ \frac{1}{\sqrt{3}}\left[2\left(n_{IJ}^{[1|7]} + n_{IJ}^{[4|6]}\right) \quad 0 \quad 0 \quad n_{IJ}^{[4|5]} + n_{IJ}^{[2|7]} \quad n_{IJ}^{[5|5]} + \frac{1}{3}n_{IJ}^{[7|7]} \quad n_{IJ}^{[5|6]} + n_{IJ}^{[3|7]}\right]^T \\ \frac{1}{\sqrt{3}}\left[0 \quad 0 \quad 2\left(n_{IJ}^{[3|7]} + n_{IJ}^{[5|6]}\right) \quad n_{IJ}^{[4|4]} + \frac{1}{3}n_{IJ}^{[7|7]} \quad n_{IJ}^{[4|5]} + n_{IJ}^{[2|7]} \quad n_{IJ}^{[4|6]} + n_{IJ}^{[1|7]}\right]^T \\ \frac{2}{3}\left[0 \quad 0 \quad 0 \quad n_{IJ}^{[4|7]} \quad n_{IJ}^{[5|7]} \quad n_{IJ}^{[6|7]}\right]^T \end{pmatrix}. \tag{B.3}$$

Here, the part of $\mathbf{n}_0^M|_{IJ}$ related to $\tilde{n}_{IJ}^{[K|7]}$ is updated using Eq. (A.6) once for each element per each increment of nonlinear solution. The remaining parts of $\mathbf{n}_0^M|_{IJ}$, and the constants $\mathbf{E}_j|_{IJ}$ $(j = 1,2,3)$, $\mathbf{n}_j^k\big|_{IJ}$ and $\mathbf{S}_j|_{IJ}$ $(j = 4, 5, 6)$ are independent of solution increments, locations within elements and are the same for all elements and hence are only calculated once.

It is possible to represent the assumed strain field in Eq. (18) in terms of nodal constants as

$$\tilde{n}_{rrIJ}^{as} = \tilde{n}_{rrIJ}^{con} + \frac{\sqrt{3}}{4}{}^0\lambda(r,s,t)s\widehat{n}_{rrIJ}^{s} + \frac{\sqrt{3}}{4}{}^0\lambda(r,s,t)t\widehat{n}_{rrIJ}^{t} + \frac{3}{4}{}^0\lambda(r,s,t)st\widehat{n}_{rrIJ}^{st},$$

$$\tilde{n}_{ssIJ}^{as} = \tilde{n}_{ssIJ}^{con} + \frac{\sqrt{3}}{4}{}^0\lambda(r,s,t)t\widehat{n}_{ssIJ}^{t} + \frac{\sqrt{3}}{4}{}^0\lambda(r,s,t)r\widehat{n}_{ssIJ}^{r} + \frac{3}{4}{}^0\lambda(r,s,t)tr\widehat{n}_{ssIJ}^{tr},$$

$$\tilde{n}_{ttIJ}^{as} = \tilde{n}_{ttIJ}^{con} + \frac{\sqrt{3}}{4}{}^0\lambda(r,s,t)r\widehat{n}_{ttIJ}^{r} + \frac{\sqrt{3}}{4}{}^0\lambda(r,s,t)s\widehat{n}_{ttIJ}^{s} + \frac{3}{4}{}^0\lambda(r,s,t)rs\widehat{n}_{ttIJ}^{rs},$$

$$\tilde{n}_{rsIJ}^{as} = \tilde{n}_{rsIJ}^{con} + \frac{1}{2}{}^0\lambda(r,s,t)t\widehat{n}_{rsIJ}^{t} + \frac{\sqrt{3}}{8}\tanh({}_0^tc)(\widehat{n}_{rsIJ}^{r}r + \widehat{n}_{rsIJ}^{s}s + \sqrt{3}\widehat{n}_{rsIJ}^{rs}rs){}^0\lambda(r,s,t),$$

$$\tilde{n}_{stIJ}^{as} = \tilde{n}_{stIJ}^{con} + \frac{1}{2}{}^0\lambda(r,s,t)r\widehat{n}_{stIJ}^{r} + \frac{\sqrt{3}}{8}\tanh({}_0^tc)(\widehat{n}_{stIJ}^{s}s + \widehat{n}_{stIJ}^{t}t + \sqrt{3}\widehat{n}_{stIJ}^{st}st){}^0\lambda(r,s,t),$$

$$\tilde{n}_{trIJ}^{as} = \tilde{n}_{trIJ}^{con} + \frac{1}{2}{}^0\lambda(r,s,t)s\widehat{n}_{trIJ}^{s} + \frac{\sqrt{3}}{8}\tanh({}_0^tc)(\widehat{n}_{trIJ}^{t}t + \widehat{n}_{trIJ}^{r}r + \sqrt{3}\widehat{n}_{trIJ}^{tr}tr){}^0\lambda(r,s,t), \tag{B.4}$$

$$\left[\tilde{n}_{rrIJ}^{con}\ \ \tilde{n}_{ssIJ}^{con}\ \ \tilde{n}_{ttIJ}^{con}\ \ \tilde{n}_{rsIJ}^{con}\ \ \tilde{n}_{stIJ}^{con}\ \ \tilde{n}_{trIJ}^{con}\right]^T = \sum_{M=1}^{9}\mathbf{C}_0^{M^T}\mathbf{n}_0^M\big|_{IJ},$$

$$\begin{bmatrix}\widehat{n}_{rrIJ}^{s}\\ \widehat{n}_{rrIJ}^{t}\\ \widehat{n}_{rrIJ}^{st}\end{bmatrix} = \begin{bmatrix}\mathbf{G}_1^2 & \mathbf{G}_1^1 & \mathbf{G}_1^4 & \mathbf{G}_1^3\\ \mathbf{G}_1^3 & \mathbf{G}_1^4 & \mathbf{G}_1^1 & \mathbf{G}_1^2\\ \mathbf{G}_1^4 & \mathbf{G}_1^3 & \mathbf{G}_1^2 & \mathbf{G}_1^1\end{bmatrix}\mathbf{E}_1|_{IJ}, \begin{bmatrix}\widehat{n}_{ssIJ}^{t}\\ \widehat{n}_{ssIJ}^{r}\\ \widehat{n}_{ssIJ}^{tr}\end{bmatrix} = \begin{bmatrix}\mathbf{G}_2^2 & \mathbf{G}_2^1 & \mathbf{G}_2^4 & \mathbf{G}_2^3\\ \mathbf{G}_2^3 & \mathbf{G}_2^4 & \mathbf{G}_2^1 & \mathbf{G}_2^2\\ \mathbf{G}_2^4 & \mathbf{G}_2^3 & \mathbf{G}_2^2 & \mathbf{G}_2^1\end{bmatrix}\mathbf{E}_2|_{IJ},$$

$$\begin{bmatrix}\widehat{n}_{ttIJ}^{r}\\ \widehat{n}_{ttIJ}^{s}\\ \widehat{n}_{ttIJ}^{rs}\end{bmatrix} = \begin{bmatrix}\mathbf{G}_3^2 & \mathbf{G}_3^1 & \mathbf{G}_3^4 & \mathbf{G}_3^3\\ \mathbf{G}_3^3 & \mathbf{G}_3^4 & \mathbf{G}_3^1 & \mathbf{G}_3^2\\ \mathbf{G}_3^4 & \mathbf{G}_3^3 & \mathbf{G}_3^2 & \mathbf{G}_3^1\end{bmatrix}\mathbf{E}_3|_{IJ}, \widehat{n}_{rsIJ}^{t} = \mathbf{G}_4^2\mathbf{n}_4^1\big|_{IJ} + \mathbf{G}_4^1\mathbf{n}_4^2\big|_{IJ},$$

$$\begin{bmatrix}\widehat{n}_{rsIJ}^{r}\\ \widehat{n}_{rsIJ}^{s}\\ \widehat{n}_{rsIJ}^{rs}\end{bmatrix} = \begin{bmatrix}\mathbf{H}_4^2 & \mathbf{H}_4^1 & \mathbf{H}_4^4 & \mathbf{H}_4^3 & \mathbf{H}_4^6 & \mathbf{H}_4^5 & \mathbf{H}_4^8 & \mathbf{H}_4^7\\ \mathbf{H}_4^3 & \mathbf{H}_4^4 & \mathbf{H}_4^1 & \mathbf{H}_4^2 & \mathbf{H}_4^7 & \mathbf{H}_4^8 & \mathbf{H}_4^5 & \mathbf{H}_4^6\\ \mathbf{H}_4^4 & \mathbf{H}_4^3 & \mathbf{H}_4^2 & \mathbf{H}_4^1 & \mathbf{H}_4^8 & \mathbf{H}_4^7 & \mathbf{H}_4^6 & \mathbf{H}_4^5\end{bmatrix}\mathbf{S}_4|_{IJ}, \widehat{n}_{stIJ}^{r} = \mathbf{G}_5^2\mathbf{n}_5^1\big|_{IJ} + \mathbf{G}_5^1\mathbf{n}_5^2\big|_{IJ},$$

$$\begin{bmatrix}\widehat{n}_{stIJ}^{s}\\ \widehat{n}_{stIJ}^{t}\\ \widehat{n}_{stIJ}^{st}\end{bmatrix} = \begin{bmatrix}\mathbf{H}_5^2 & \mathbf{H}_5^1 & \mathbf{H}_5^4 & \mathbf{H}_5^3 & \mathbf{H}_5^6 & \mathbf{H}_5^5 & \mathbf{H}_5^8 & \mathbf{H}_5^7\\ \mathbf{H}_5^3 & \mathbf{H}_5^4 & \mathbf{H}_5^1 & \mathbf{H}_5^2 & \mathbf{H}_5^7 & \mathbf{H}_5^8 & \mathbf{H}_5^5 & \mathbf{H}_5^6\\ \mathbf{H}_5^4 & \mathbf{H}_5^3 & \mathbf{H}_5^2 & \mathbf{H}_5^1 & \mathbf{H}_5^8 & \mathbf{H}_5^7 & \mathbf{H}_5^6 & \mathbf{H}_5^5\end{bmatrix}\mathbf{S}_5|_{IJ}, \widehat{n}_{trIJ}^{s} = \mathbf{G}_6^2\mathbf{n}_6^1\big|_{IJ} + \mathbf{G}_6^1\mathbf{n}_6^2\big|_{IJ},$$

$$\begin{bmatrix}\widehat{n}_{trIJ}^{t}\\ \widehat{n}_{trIJ}^{r}\\ \widehat{n}_{trIJ}^{tr}\end{bmatrix} = \begin{bmatrix}\mathbf{H}_6^2 & \mathbf{H}_6^1 & \mathbf{H}_6^4 & \mathbf{H}_6^3 & \mathbf{H}_6^6 & \mathbf{H}_6^5 & \mathbf{H}_6^8 & \mathbf{H}_6^7\\ \mathbf{H}_5^3 & \mathbf{H}_6^4 & \mathbf{H}_6^1 & \mathbf{H}_6^2 & \mathbf{H}_6^7 & \mathbf{H}_6^8 & \mathbf{H}_6^5 & \mathbf{H}_6^6\\ \mathbf{H}_5^4 & \mathbf{H}_6^3 & \mathbf{H}_6^2 & \mathbf{H}_6^1 & \mathbf{H}_6^8 & \mathbf{H}_6^7 & \mathbf{H}_6^6 & \mathbf{H}_6^5\end{bmatrix}\mathbf{S}_6|_{IJ}. \tag{B.5}$$

In Eq. (B.4), we carry out the computations that depend on the natural coordinates (r, s, t) (for each Gauss point), once for each different nodal coupling (nodes I and J). Using Eqs. (B.2) and (B.3) to Eq. (B.5), we calculate (once per each element) the constants $\widehat{n}_{kkIJ}^{i}$, $\widehat{n}_{kkIJ}^{j}$, $\widehat{n}_{kkIJ}^{ij}$, $\widehat{n}_{ijIJ}^{k}$, $\widehat{n}_{ijIJ}^{i}$, $\widehat{n}_{ijIJ}^{j}$ and $\widehat{n}_{ijIJ}^{ij}$, and update $\tilde{n}_{ijIJ}^{con}$ in each increment.

The nodal constants for the global volumetric and deviatoric strains ($\overline{n}_{IJ}^{vol}$ and $\overline{n}_{ijIJ}^{dev}$) are obtained from

$$\overline{n}_{IJ}^{vol} = \overline{n}_{xxIJ}^{dil} + \overline{n}_{yyIJ}^{dil} + \overline{n}_{zzIJ}^{dil}, \overline{n}_{ijIJ}^{dev} = \overline{n}_{ijIJ}^{as} - \frac{1}{3}\overline{n}_{IJ}^{vol}\delta_{ij},$$

$$\overline{n}_{ijIJ}^{as} = \tilde{n}_{klIJ}^{as}(\mathbf{i}_i \cdot {}^0\widehat{\mathbf{g}}^k)(\mathbf{i}_j \cdot {}^0\widehat{\mathbf{g}}^l), \overline{n}_{iiIJ}^{dil} = \tilde{n}_{klIJ}^{con}(\mathbf{i}_i \cdot {}^0\widehat{\mathbf{g}}^k)(\mathbf{i}_j \cdot {}^0\widehat{\mathbf{g}}^l). \tag{B.6}$$

The deviatoric strain-displacement matrices ($\overline{\mathbf{B}}_{ij}^{dev}$ and $\overline{\mathbf{N}}_{ij}^{dev}$) are obtained by

$$\overline{\mathbf{B}}_{ij}^{dev} = \left(\overline{\mathbf{B}}_{ij1}^{dev} \ \cdots\ \overline{\mathbf{B}}_{ijI}^{dev} \ \cdots\ \overline{\mathbf{B}}_{ij8}^{dev}\right), \overline{\mathbf{B}}_{ijI}^{dev} = \sum_{J=1}^{8}\begin{pmatrix}\overline{n}_{ijIJ}^{devt}x_J & 0 & 0\\ 0 & \overline{n}_{ijIJ}^{devt}y_J & 0\\ 0 & 0 & \overline{n}_{ijIJ}^{devt}z_J\end{pmatrix},$$

$$\overline{\mathbf{N}}_{ij}^{dev} = \begin{pmatrix}\overline{\mathbf{N}}_{ij11}^{dev} & \cdots & \overline{\mathbf{N}}_{ij18}^{dev}\\ \vdots & \overline{\mathbf{N}}_{ijIJ}^{dev} & \vdots\\ \overline{\mathbf{N}}_{ij81}^{dev} & \cdots & \overline{\mathbf{N}}_{ij88}^{dev}\end{pmatrix}, \overline{\mathbf{N}}_{ijIJ}^{dev} = \overline{n}_{ijIJ}^{dev}\begin{pmatrix}1 & 0 & 0\\ 0 & 1 & 0\\ 0 & 0 & 1\end{pmatrix}, \tag{B.7}$$

where similar relation also holds for volumetric strain-displacement matrices, $\overline{\mathbf{B}}^{vol}$ and $\overline{\mathbf{N}}^{vol}$ with $\overline{n}_{IJ}^{vol}$.

References

[1] Bathe KJ. Finite element procedures. Prentice Hall; 1996, 2nd ed. K.J. Bathe, Watertown, MA; 2014 and Higher Education Press, China; 2016.

[2] Bathe KJ. The inf–sup condition and its evaluation for mixed finite element methods. Comput Struct 2001;79(2):243–52.

[3] Wilson EL, Ibrahimbegovic A. Use of incompatible displacement modes for the calculation of element stiffnesses or stresses. Finit Elem Anal Des 1990;7(3):229–41.

[4] Simo JC, Rifai MS. A class of mixed assumed strain methods and the method of incompatible modes. Int J Numer Meth Eng 1990;29(8):1595–638.

[5] Kasper EP, Taylor RL. A mixed-enhanced strain method: part I: geometrically linear problems. Comput Struct 2000;75(3):237–50.

[6] Alves de Sousa RJ, Natal Jorge RM, Fontes Valente RA, César de Sá JMA. A new volumetric and shear locking-free 3D enhanced strain element. Eng Comput 2003;20(7):896–925.

[7] Wriggers P, Reese S. A note on enhanced strain methods for large deformations. Comp Meth Appl Mech Eng 1996;135(3–4):201–9.

[8] Sussman T, Bathe KJ. Spurious modes in geometrically nonlinear small displacement finite elements with incompatible modes. Comput Struct 2014;140:14–22.

[9] Korelc J, Wriggers P. Consistent gradient formulation for a stable enhanced strain method for large deformations. Eng Comput 1996;13(1):103–23.

[10] Pantuso D, Bathe KJ. On the stability of mixed finite elements in large strain analysis of incompressible solids. Finit Elem Anal Des 1997;28(2):83–104.

[11] Reese S, Küssner M, Reddy BD. A new stabilization technique for finite elements in non-linear elasticity. Int J Numer Meth Eng 1999;44(11):1617–52.

[12] Wall WA, Bischoff M, Ramm E. A deformation dependent stabilization technique, exemplified by EAS elements at large strains. Comp Meth Appl Mech Eng 2000;188(4):859–71.

[13] Bischoff M, Bletzinger KU. Interaction of locking and element stability at large strains. In: VIII international conference on computational plasticity. Barcelona; 2005.

[14] Korelc J, Šolinc U, Wriggers P. An improved EAS brick element for finite deformation. Comp Mech 2010;46(4):641–59.

[15] Dvorkin EN, Bathe KJ. A continuum mechanics based four-node shell element for general non-linear analysis. Eng Comput 1984;1(1):77–88.

[16] Radovitzky RA, Dvorkin EN. A 3D element for non-linear analysis of solids. Int J Numer Meth Bio Eng 1994;10(3):183–94.

[17] Lee PS, Bathe KJ. Development of MITC isotropic triangular shell finite elements. Comput Struct 2004;82(11):945–62.
[18] Bucalem ML, Bathe KJ. The mechanics of solids and structures – hierarchical modeling and the finite element solution. Springer; 2011.
[19] Lee Y, Lee PS, Bathe KJ. The MITC3+ shell element and its performance. Comput Struct 2014;138:12–23.
[20] Ko Y, Lee PS, Bathe KJ. A new 4-node MITC element for analysis of two-dimensional solids and its formulation in a shell element. Comput Struct 2017;192:34–49.
[21] Sussman T, Bathe KJ. A finite element formulation for nonlinear incompressible elastic and inelastic analysis. Comput Struct 1987;26(1–2):357–409.
[22] ADINA R & D, Inc. ADINA Theory and Modeling Guide; 2017 <http://www.adina.com>.
[23] MacNeal RH, Harder RL. A proposed standard set of problems to test finite element accuracy. Finit Elem Anal Des 1985;1(1):3–20.
[24] Chen XM, Cen S, Long YQ, Yao ZH. Membrane elements insensitive to distortion using the quadrilateral area coordinate method. Comput Struct 2004;82(1):35–54.
[25] Cen S, Chen XM, Fu XR. Quadrilateral membrane element family formulated by the quadrilateral area coordinate method. Comp Meth Appl Mech Eng 2007;196(41):4337–53.
[26] Li HG, Cen S, Cen ZZ. Hexahedral volume coordinate method (HVCM) and improvements on 3D Wilson hexahedral element. Comp Meth Appl Mech Eng 2008;197(51):4531–48.
[27] Hiller JF, Bathe KJ. Measuring convergence of mixed finite element discretizations: an application to shell structures. Comput Struct 2003;81(8):639–54.
[28] Chapelle D, Bathe KJ. The finite element analysis of shells – fundamentals, 1st ed. Springer; 2003; 2nd ed. Springer; 2011.
[29] Bathe KJ, Lee PS, Hiller JF. Towards improving the MITC9 shell element. Comput Struct 2003;81(8):477–89.